The two-component regulator WalKR provides an essential link between cell wall homeostasis with DNA replication in *Staphylococcus aureus*

Liam K. R. Sharkey[1], Romain Guerillot[1], Calum Walsh[1], Adrianna M. Turner[1], Jean Y. H. Lee[1], Stephanie L. Neville[1], Stephan Klatt[2], Sarah L. Baines[1], Sacha Pidot[1], Fernando J. Rossello[3,4], Torsten Seemann[1,5], Hamish McWilliam[1], Ellie Cho[6], Glen P. Carter[1], Benjamin P. Howden[1,5], Christopher A. McDevitt[1], Abderrahman Hachani[1], Timothy P. Stinear[1,5,*] and Ian R. Monk[1,*]

1. Department of Microbiology and Immunology, Doherty Institute for Infection and Immunity, University of Melbourne, Melbourne, Victoria, 3000, Australia
2. The Florey Institute of Neuroscience and Mental Health, Melbourne Dementia Research Centre, The University of Melbourne, Parkville, Victoria, 3010, Australia.
3. University of Melbourne Centre for Cancer Research, The University of Melbourne, Melbourne, Victoria, 3000, Australia.
4. Australian Regenerative Medicine Institute, Monash University, Melbourne, Victoria, 3800, Australia.
5. Centre for Pathogen Genomics, Department of Microbiology and Immunology, Doherty Institute for Infection and Immunity, University of Melbourne, Melbourne, Victoria, 3000, Australia
6. Biological Optical Microscopy Platform, University of Melbourne, Melbourne, Victoria, 3000, Australia

* Joint senior authors

Abstract

Among the 16 two-component systems (TCSs) in the opportunistic human pathogen *Staphylococcus aureus*, only WalKR is essential. Like orthologous systems in other Bacillota, *S. aureus* WalKR controls autolysins involved in peptidoglycan remodelling and is therefore intimately involved in cell division. However, despite the importance of WalKR in *S. aureus*, the basis for its essentiality is not understood and the regulon poorly defined. Here, we defined a consensus WalR DNA-binding motif and the direct WalKR regulon by using functional genomics, including ChIP-seq, with a panel of isogenic *walKR* mutants that had a spectrum of altered activities. Consistent with prior findings, the direct regulon includes multiple autolysin genes. However, this work also revealed that WalR directly regulates at least five essential genes involved in lipoteichoic acid synthesis (*ltaS*); translation *(rplK*); DNA compaction (*hup*); initiation of DNA replication (*dnaA, hup*); and purine nucleotide metabolism (*prs*). Thus, WalKR in *S. aureus* serves as a polyfunctional regulator that contributes to fundamental control over critical cell processes by co-ordinately linking cell wall homeostasis with purine biosynthesis, protein biosynthesis, and DNA replication. Collectively, our findings address the essentiality of this locus and highlight the importance of WalKR as a *bona fide* target for novel anti-staphylococcal therapeutics.

41 ## Introduction

42 *Staphylococcus aureus* is an opportunistic pathogen that causes a wide range of hospital and
43 community acquired infections. Antibiotic-resistant strains, notably methicillin resistant
44 (MRSA) and vancomycin-intermediate (VISA) strains, are persistent problems, with last-line
45 agents, such as vancomycin, linezolid, and daptomycin, commonly associated with treatment
46 failure [1, 2]. MRSA is a World Health Organization "priority antibiotic-resistant pathogen" for
47 the research and development of new antibiotics. Mortality from serious *S. aureus* infection
48 is high (20 - 50% of bacteraemias) [3], and the socioeconomic burden of *S. aureus* disease is
49 substantial [4].

50 *S. aureus* encodes 16 core genome two-component systems (TCSs) that allow the
51 bacterium to sense and respond to a range of stimuli, providing regulatory flexibility in
52 changing environments. Of these 16 TCSs, only WalKR is essential for cell viability under
53 laboratory conditions [5, 6, 7, 8]. WalKR is a canonical TCS that is conserved amongst low-GC
54 Gram-positive bacteria, comprised of a multi-domain transmembrane sensor histidine kinase
55 (WalK) and DNA binding response regulator (WalR) of the OmpR family [9, 10]. Upon activation
56 by signal(s) WalK auto-phosphorylates a conserved histidine residue (H385) and subsequently
57 transfers the phosphoryl group to a conserved aspartate residue (D53) in WalR.
58 Phosphorylated WalR binds to promoter regions of genes within the WalKR regulon,
59 operating as either a transcriptional activator or repressor.

60 WalKR is a master regulator of cell wall homeostasis through the control of a suite of
61 autolysins [7, 11, 12, 13]. Although the locus is highly conserved, several points of difference
62 between bacterial genera suggest variation in the precise cellular function of the system and

63 the associated mechanism(s) of the essentiality. WalKR is located within an operon of three
64 to six genes that also includes a varying number of accessory factors. Two accessory genes,
65 *yycH* and *yycI* encode membrane associated proteins that differ in their function across
66 genera. In *S. aureus*, these proteins are activators of WalKR activity, while conversely in
67 *Bacillus subtilis* they are repressors [14, 15]. A second key difference between the systems is how
68 WalKR interacts with the division septum. In *B. subtilis*, WalK controls the expression of FtsZ
69 [16], it is localised to the division septum in an FtsZ dependent manner and interacts with
70 proteins of the divisome. Consequently, WalKR essentiality in *B. subtilis* arises from the co-
71 ordination of cell wall remodelling with cell division, in response to signalling via an
72 extracellular Per Arnt Sim (PAS) domain [17, 18, 19, 20]. In *S. aureus*, WalK is also reported to localise
73 to the division septum in growing cells [21]. Despite this, there remains no evidence of
74 interaction with proteins of the divisome and FtsZ has not been mapped to the staphylococcal
75 WalKR regulon. WalKR depleted *S. aureus* can be complemented with constitutively
76 overexpressed autolysins *lytM* or *ssaA* to restore bacterial viability. However, the resultant
77 cells have morphological defects and neither of these genes are themselves essential [6]. The
78 *B. subtilis* extracellular PAS domain of WalK senses peptidoglycan cleavage products
79 generated by WalKR regulated autolysins, leading to homeostatic control of cell wall
80 remodelling [22]. The signal sensed by the extracellular PAS domain in *S. aureus* is not known.
81 However, WalK activity in staphylococci (and predicted in enterococci), but not in other
82 bacillota, is modulated through co-ordination of a divalent metal ion by an intracellular PAS
83 domain [23], raising the possibility of differing roles in regulation beyond peptidoglycan
84 biosynthesis in these genera.

85 The WalKR regulon in *S. aureus* has been determined by comparative transcriptomics
86 by depleting WalKR [7, 12] or by the expression a constitutively active WalR phosphomemetic
87 amino acid substitution (D53E) [24, 25]. These studies, coupled with motif searching using a WalR
88 DNA binding motif defined in *B. subtilis* [11] have built a partial map of the WalKR regulon that
89 includes genes involved in cell wall homeostasis [7, 12] and virulence [24]. Here, we applied a
90 customised implementation of chromatin immunoprecipitation sequencing (ChIP-seq), to
91 define a 17 bp *S. aureus* WalR consensus-binding motif and identify regulation of a number
92 of essential genes involved in lipoteichoic acid polymerisation, ribosome biogenesis, purine
93 nucleotide salvage/de novo synthesis and DNA replication. These data connect the regulation
94 of cell division with chromosomal replication in *S. aureus* for the first time and identify
95 pathways outside the regulation of autolysins to explain the essentiality of WalKR.

96

97 ## Results

98 **Specific mutations in the *walKR* locus increase and decrease WalKR activity.**

99 We initially assembled a panel of isogenic mutants with altered WalK or WalR activity in the
100 native context to understand regulation without under- or over-expression. These included
101 two previously described 'down' mutants with decreased WalKR activity; *S. aureus* NRS384
102 Δ*yycHI*, with the deletion of both WalKR auxiliary proteins (*yycH* and *yycI*) [14], and NRS384
103 $WalR_{T101A}$, in which second site PknB phosphorylation at residue T101 was abolished [26]. We
104 also selected two 'up' mutants that have increased WalKR activity; NRS384 $WalK_{Y32C}$ with a
105 mutation in the first transmembrane domain (identified from a sectored Δ*yycHI* colony [23]),
106 and NRS384 $WalK_{T389A}$ that is predicted to prevent the dephosphorylation of WalR [27].

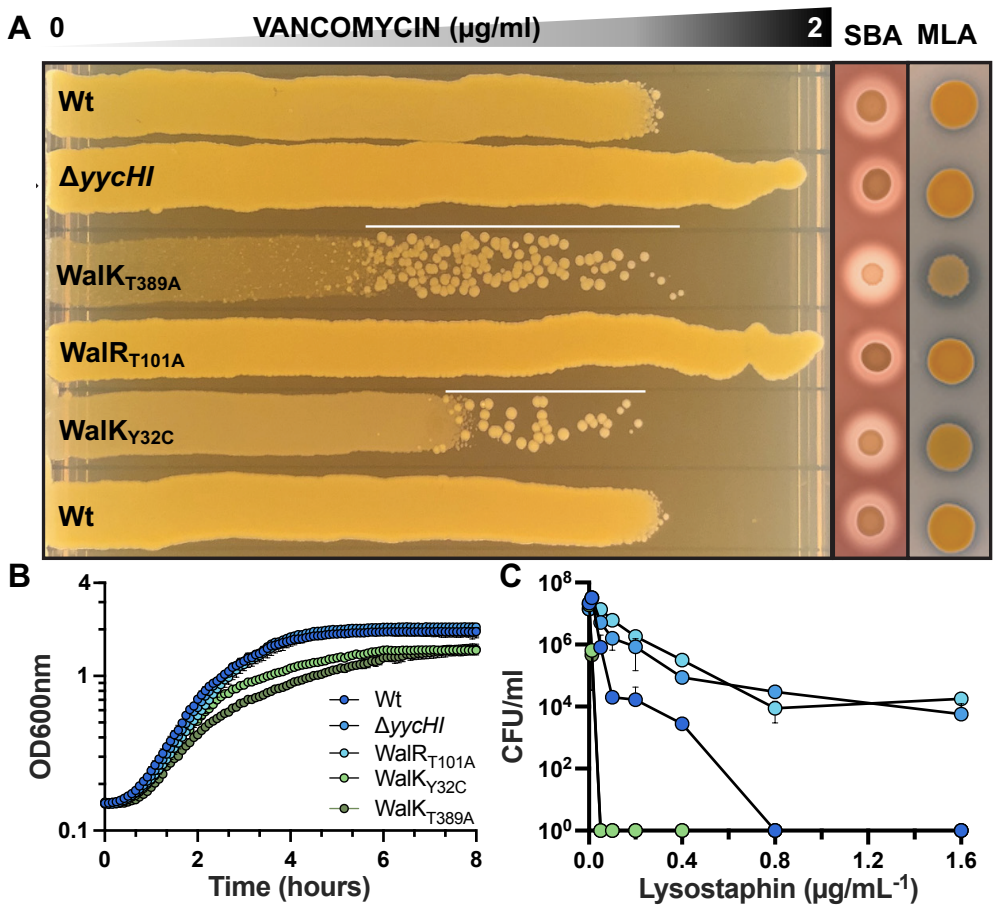

D

MIC (µg/mL^{-1})	Wt	Δ*yycHI*	WalK$_{Y32C}$	WalR$_{T101A}$	WalK$_{T389A}$
Ciprofloxacin	2	2	2	2	2
Erythromycin	1	2	1	2	1
Lincomycin	4	4	4	4	4
Trimethoprim	4	2	4	4	4
Oxacillin	64	64	4	64	0.5
Tunicamycin	≥32	≥32	0.125	≥32	0.125

Figure 1. Phenotypic characterisation of WalKR mutant strains. *A) Vancomycin gradient assay (VGA), sheep blood agar (SBA) Micrococcus luteus agar (MLA) for the comparison of vancomycin susceptibility, haemolysis and Atl mediated autolytic activity, respectively. White line on VGA plates highlights suppressor mutants that arise from exposure to vancomycin in the 'up' mutants. B) Growth curves, C) Susceptibility to lysostaphin after a 90 min exposure and D) Minimal inhibitory concentration of antibiotics against the different WalKR mutant strains, with differences to NRS384 Wt highlighted.*

107 We then confirmed that each mutant exhibited the expected phenotypes with 'up'
108 mutations resulting in an increased susceptibility to vancomycin and lysostaphin, increased

109 haemolysis, reduced growth rate, and increased autolysis with the opposite true for 'down'
110 mutants [Figure 1A-C] [12, 24, 28]. Of the two 'up' mutants, $WalK_{T389A}$ showed the most prominent
111 differences, suggesting the higher level of activation [Figure 1A-C]. Mutational activation of
112 WalKR caused a striking increase in susceptibility to oxacillin and tunicamycin, eliciting >16-
113 fold changes in susceptibility to these cell wall targeting agents. Conversely, mutational
114 dampening of WalKR activity caused a small but reproducible (2-fold) decrease in
115 erythromycin susceptibility, but we did not observe erythromycin or lincomycin
116 hypersensitivity upon WalKR modulation as has previously been reported [5, 29]. Susceptibility
117 to compounds targeting other cellular pathways remained unchanged [Figure 1D].

118 TCS phosphoryl transfer from the sensor histidine kinase to the cognate DNA-binding
119 response regulator requires direct interaction [30]. To assess the impact of the 'up' and 'down'
120 mutations on interaction dynamics between WalK and WalR across growth, we implemented
121 a split luciferase system [31]. Proteins were C-terminally tagged (separated by a glycine serine
122 linker) with either the small bit (SmBIT- 11 amino acids) or large bit (LgBIT – 17.6 kDa) to

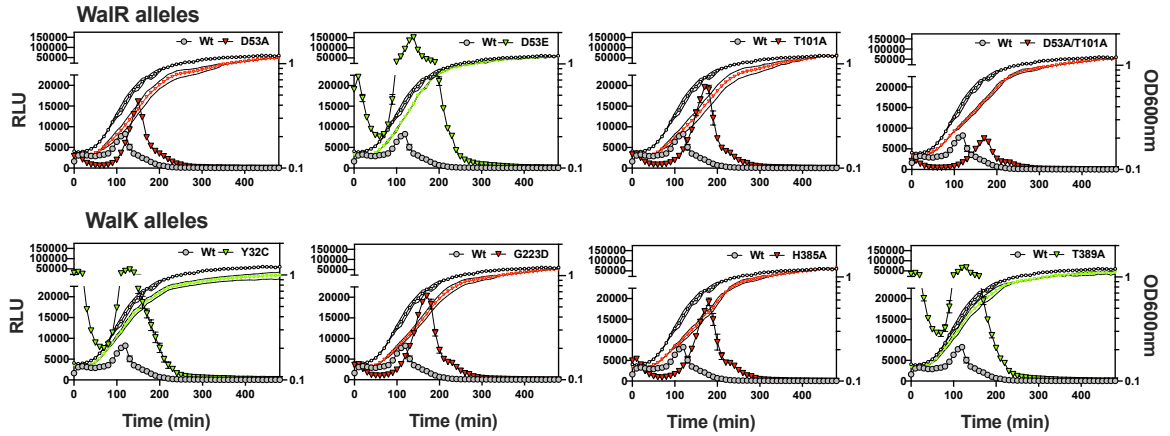

Figure 2. Kinetic interaction of WalR with WalK in S. aureus*. Analysis of the interaction of WalR-SmBIT with WalK-LgBIT and WalK/WalR mutant proteins throughout growth in NRS384 Wt. OD600nm: open black circle (WalR/WalK Wt) and open red triangle ('down' mutant) or open green triangle ('up' mutant). RLU: grey filled circle (WalR/WalK Wt) and either red ('down' mutation) or green ('up' mutation) filled triangle. Results are the mean from three independent determinations and the error bars show the standard deviation.*

123 reconstitute a functional luciferase that emits light in the presence of the furimazine
124 substrate. Our modifications allowed the kinetics of protein-protein interaction to be non-
125 invasively measured throughout *S. aureus* growth. Chromosomal C-terminal tagging of WalR-
126 SmBIT and WalK-LgBIT at the native locus showed that the proteins tolerated the presence of
127 either tag, with no growth defect detected [Figure S1].

128 We then constructed WalR-SmBIT and WalK-LgBIT fusions in the plasmid system with
129 native and mutant proteins, following cell density (OD600nm) and light emission (RLU)
130 throughout *S. aureus* growth. We observed immediate interaction of WalK with WalR upon
131 dilution in fresh LB with the peak interaction in the mid-exponential phase of growth, and
132 subsequent rapid decline of the interaction to undetectable levels (5 h) in stationary phase.
133 This pattern of interaction was enhanced in the 'up' mutant strains throughout growth
134 (including lag phase) for both $WalK_{Y32C}$, $WalK_{T389A}$, and the previously described $WalR_{D53E}$
135 mutant [24, 25] compared to the native WalK/WalR interaction [Figure 2]. In contrast, the 'down'
136 mutants strains, which included $WalR_{D53A}$ (cannot be phosphorylated by WalK), $WalR_{T101A}$,
137 $WalK_{D53A/T101A}$, and $WalK_{G223D}$ (reduced autophosphorylation and transfer to WalR [32]),
138 exhibited a consistent profile of reduced initial WalK/WalR interaction during lag phase in
139 comparison to the native WalK/WalR alleles [Figure 2]. The kinetic profile of the $WalR_{T101A}$
140 mutant mimicked the interaction profile of the $WalK_{G223D}$ mutant with a 1.5-fold increase in
141 the maximal level of interaction (compared to native WalK/WalR). This increase correlated
142 with the same mid-log phase time point as seen in the native interaction [Figure 2]. 'Down'
143 mutants also yielded detectable interaction into stationary phase. These interaction profiles
144 combined with phenotypic profiling validate our panel of 'up' and 'down' mutants.

145 **WalKR activation causes a global change in gene expression**

146 To ascertain the impact of WalKR activation on *S. aureus* gene expression we compared the
147 transcriptome of 'up' mutant $WalK_{T389A}$ to the NRS384 strain. Activation of WalKR was
148 associated with a global gene expression change, wherein ~55% of genes (1,117) were
149 significant (False Discovery Rate (FDR) $\leq$0.05, $log_2FC \geq 0.585$) with approximately half (551) up-
150 regulated and half (564) down-regulated [Figure 3C]. Genes with increased expression (≥1.5
151 log_2FC, FDR $\leq$0.05) included those encoding autolysins, virulence factors, membrane
152 transporters, and proteins of the amino acid, purine, and fatty acid biosynthesis pathways

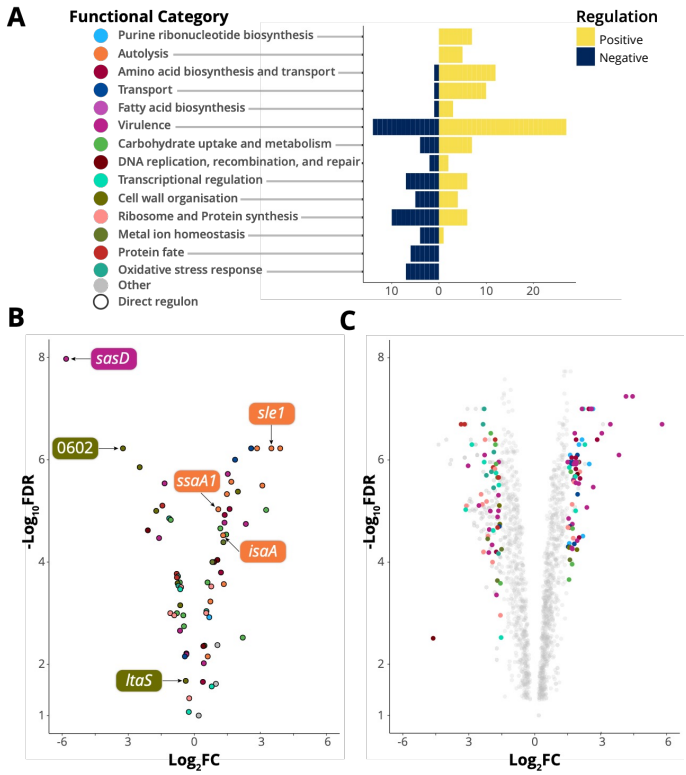

Figure 3. The direct and indirect WalKR regulon. *A) The number of genes in each category that is positively or negatively regulated upon WalK activation (FDR $\leq$0.05, $log_2FC \geq 1.5$ or $\leq$-1.5). For clarity, categories where n $\leq$ 2 are not shown B) Gene expression changes of the predicted direct WalKR regulon upon WalK activation (Wt vs $WalK_{T389A}$). Genes with WalR binding sites confirmed by ChIP-seq are highlighted (see Figure 4D and Table S1). C) Global change in transcriptome upon mutational activation of WalK (Wt vs $WalK_{T389A}$), members of gene sets undergoing a $log_2FC \geq 1.5$ or $\leq$-1.5 are highlighted. Y-axis labels in panel A serve as the legend for panels B and C.*

153 [Figure 3A, Table S1]. Genes with decreased expression ($log_2FC \leq -1.5$, FDR ≤ 0.05) were
154 primarily involved in oxidative stress response, metal ion homeostasis, and protein fate
155 [Figure 3A, Table S1]. Whereas the expression of genes encoding ribosomal proteins,
156 transcription factors, and proteins involved in carbohydrate metabolism, DNA maintenance,
157 and cell wall organisation were both up- and down-regulated (FDR ≤ 0.05, $log_2FC \geq 1.5$ or $\leq$-
158 1.5) [Figure 3A, Table S1].

159 Explanations for two of our observed WalKR phenotypes can be inferred in the
160 $WalK_{T389A}$ RNA-seq data. Firstly, increased haemoylsis [Figure 1A] in $WalK_{T389A}$ mutants is
161 explained by an increase in *hla* expression (+1.7-log_2FC), encoding alpha-toxin, upon WalK
162 activation. Secondly, enhanced zones of clearing surrounding $WalK_{T389A}$ on heat killed
163 *Micrococcus luteus* agar plates [Figure 1A] arise due to increased peptidoglycan degradation
164 of secreted processed Atl by the dual activity autolysin Atl [33] (+2.85 -log_2 FC).

165 **Defining an *in vivo* WalR regulon using ChIP-seq**

166 The direct regulon of WalR was then investigated using ChIP-seq. To permit
167 immunoprecipitation, a 1xFLAG-tag was incorporated onto the C-terminus of WalR using a
168 modified anhydrotetracycline (aTc) inducible expression plasmid [34]. To validate functionally,
169 the transcriptome of a strain *S. aureus* NRS384 with chromosomally C-terminally FLAG tagged
170 WalR [23] was compared to the wild type (Wt) strain. This strain had a gene expression profile
171 that was like NRS384 Wt during mid-log phase, as determined by RNA-seq (no significant
172 changes in gene expression (0.585 Log_2FC, 0.05 false discovery rate [FDR]). Subsequently,
173 FLAG-tagged expression constructs were also made in pRAB11 for three other response
174 regulators with known DNA-binding motifs, HptR, and SaeR, and VraR [Figure 4A] [35, 36, 37]. The
175 four plasmids and an empty vector control were each transformed into the CA-MRSA USA300

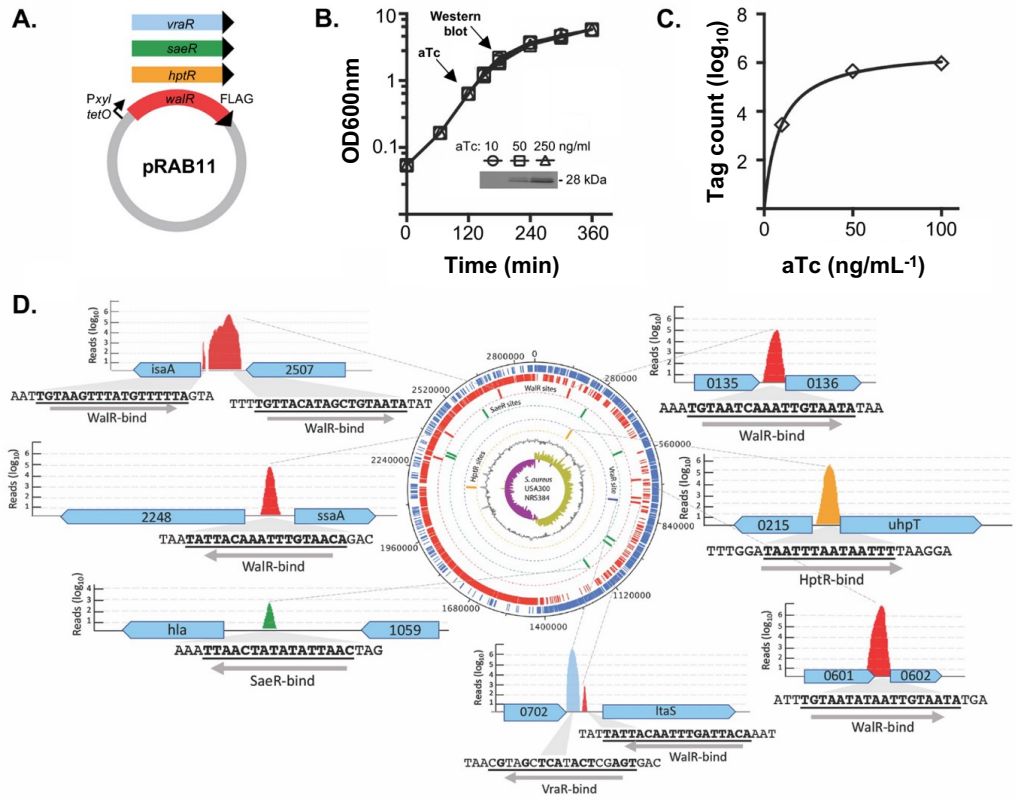

Figure 4. ChIP-seq analysis of S. aureus WalR chromosome binding sites. *A) Four response regulators with a C-terminal FLAG-tag for immunoprecipitation after induction with anhydrotetracycline (aTc) in NRS384Δspa. B) Dose dependent production of WalR-FLAG (inset Western blot) with increasing concentrations of aTc. C) Plot showing an increasing number of WalR ChIP-seq mapped reads (Tag count) as the aTc concentration increases. D) Summary of key ChIP-seq binding sites across the S. aureus chromosome, showing binding motif and direction, including five WalR peaks (red), and single peaks for SaeR (green), VraR (blue) and HptR (yellow).*

strain NRS384 with *spa*, which encodes Protein A, deleted to reduce non-specific IgG-binding. Dose-dependent aTc induction was observed (induced at an optical density of 600 nm (OD600nm) = 0.6 for 1 h) for *walR* [Figure 4B]. We examined the impact of increasing aTc concentrations on tag-counts (mapped sequence reads for ChIP purified DNA) and selected an aTc concentration of 100 ng•mL^{-1} for subsequent ChIP-seq experiments [Figure 4C]. ChIP-seq was then conducted with each of the four constructs and the empty vector. Initial analysis of the resulting sequence reads revealed a high background of reads mapping across the

183 entire *S. aureus* chromosome. To improve the signal-to-noise ratio for each of the four ChIP-
184 seq experiments, we performed *in silico* subtraction of the read sets for the three non-target
185 response-regulators and the empty vector from the read set for the target response-regulator
186 [Figure S2, Table S2]. This revealed peaks anticipated for HptR and SaeR, upstream of *hpt* and
187 *hla*, respectively [Figure 4D, Table S1], and identified WalR binding sites upstream of six genes
188 that included autolysins SAUSA300_2249 (*ssaA*), SAUSA300_2506 (*isaA*), SAUSA300_0438
189 (*sle1*), cell wall cross-linked SAUSA300_0136 (*sasD*), hypothetical secreted SAUSA300_0602,
190 and SAUSA300_0703 (*ltaS*) which encodes the essential lipoteichoic acid (LTA) synthase
191 responsible for polymerising glycerol-6-phosphate into LTA chains [38] [Figure 4D, Table S1]. All
192 these genes had previously been identified as belonging to the WalKR regulon [7, 24]. For VraR,
193 we observed a ChIP-seq binding site upstream of *ltaS*, that was adjacent to the putative WalR-
194 binding site [Figure 4D].

195 Including the above six genes (seven peaks), a total of 22 WalR ChIP-seq peaks
196 upstream of 21 genes were identified, with 12 set aside due to small peak size (7-20
197 nucleotides) and poor peak prediction scores. Two peaks were identified in 16S rRNA genes,
198 but the use of ribosomal RNA depletion precluded interpretation of RNA-seq data for these
199 loci. The peak upstream of SAUSA300_0681 was not pursued, as no candidate WalR binding
200 sites were identified (Table S1].

201 The high stringency required for the *in-silico* subtraction approach could eliminate
202 peaks corresponding to lower affinity DNA binding regions and thereby obscure the
203 identification across the breadth of the direct WalR regulon. Consequently, we used ChIP-seq
204 defined WalR binding regions in conjunction with previously validated WalR binding sites [12,
205 24] to generate a 17 bp consensus *S. aureus* WalR-binding motif (5'-TGTHH[N]$_6$WGTNDD-3')
206 [Figure S3 AB]. This motif was the used to conduct an *in-silico* search of the genome for

207 potential WalR binding sites. In total, 118 putative intergenic WalR binding sites were
208 identified within the NRS384 chromosome [Figure S2B], of which 109 were within 500 bp of
209 a predicted CDS transcriptional start site [Table S3].

210 **Positioning of WalR binding site, not sequence or orientation, dictates of mode of**
211 **regulation.**

212 To investigate whether the sequence of WalR motifs could determine the mode, or degree,
213 of change in gene expression upon activation, WalR motif diversity was visualised as a
214 maximum-likelihood phylogenetic tree and the tips labelled with gene expression changes
215 upon WalK activation [Figure S4]. Functional groups of regulated genes were also mapped to
216 examine whether specific motif signatures were linked to gene sets [Figure S5]. We did not
217 observe clustering of positively or negatively regulated genes, nor did branches of the tree
218 correspond to specific gene functions [Figure S4]. Taken together, these analyses indicate that
219 the sequence of WalR motifs does not dictate the mode of regulation, nor is it linked to the
220 functional class of the gene it controls.

221 Here, building on framework used to analyse WalR in *B. subtilis* [13], we mapped the
222 positions of *S. aureus* WalR binding sites of the direct regulon in relation to predicted
223 transcriptional start sites and promoters [39] [Table S4]. The orientation of WalR binding site in
224 relation to the downstream gene was not significantly associated with the magnitude
225 (Student's t test, $p=0.52$) or mode ($p=0.81$) of expression change. However, the position of
226 the WalR binding site did dictate the mode of regulation; WalR binding upstream of the -35
227 element was significantly associated with positive regulation ($p < 0.001$), whereas WalR
228 binding between, or downstream of, -35 and -10 elements was associated with negative
229 regulation ($p < 0.001$) [Table S4]. Thus, whether WalR activates or represses the expression

230 of a gene is determined primarily by its position relative to the promoter rather than motif
231 sequence.

232 **Functional validation of WalR directly regulated genes**

233 WalR binding to promoters of the six loci identified by ChIP-seq was assessed *in vitro*
234 using electrophoretic mobility shift assays (EMSAs) with recombinant WalR [Figure 5A, Figure
235 S5]. We observed WalR binding to all six promoters identified by ChIP-seq, with specificity
236 confirmed through competition experiments with excess labelled or unlabelled DNA duplexes
237 [Figure S6]. We also corroborated VraR binding to the *ltaS* promoter at the consensus VraR
238 binding motif (5'-TGA[N_{1-3}]TCA-3')[35, 40] [Figure S7A], while WalR had no affinity for this duplex
239 [Figure S7B]. VraR did exhibit affinity for the WalR binding site duplex, however, this was
240 shown to be non-specific by competition assay [Figure S7C]. Therefore, WalR and VraR bound
241 to the *ltaS* promoter at discrete sites dictated by their respective recognition motifs.

242 Following the *in vitro* confirmation of WalR binding to sites identified by ChIP-seq, we
243 sought to assess the impact of WalR binding on promoter activity in *S. aureus* [Figure 5B]. The
244 promoter regions encompassing the WalR binding motif were transcriptionally fused with
245 yellow fluorescent protein (YFP). To assess the impact of WalR activity on gene expression,
246 each construct and a paired WalR binding motif mutant (first TGT in WalR motif mutated to
247 CCC) was transformed into NRS384. Additionally, the native promoter construct was
248 transformed into NRS384 'down' mutant (Δ*yycHI*) and 'up' mutant ($WalK_{Y32C}$). The $WalK_{Y32C}$
249 strain was chosen rather than $WalK_{T389A}$ as suppressor mutants arose in this background
250 through genetic instability, which was not observed in $WalK_{Y32C}$. As a positive control, we
251 included the promoter for the *hpt gene* encoding the glucose-6-phosphate transporter which
252 is responsive to the presence of glucose-6-phosphate [37] [Figure 5B]. Strains were grown to
253 stationary phase with fluorescence and colony forming units determined. All of the RNA-seq
254

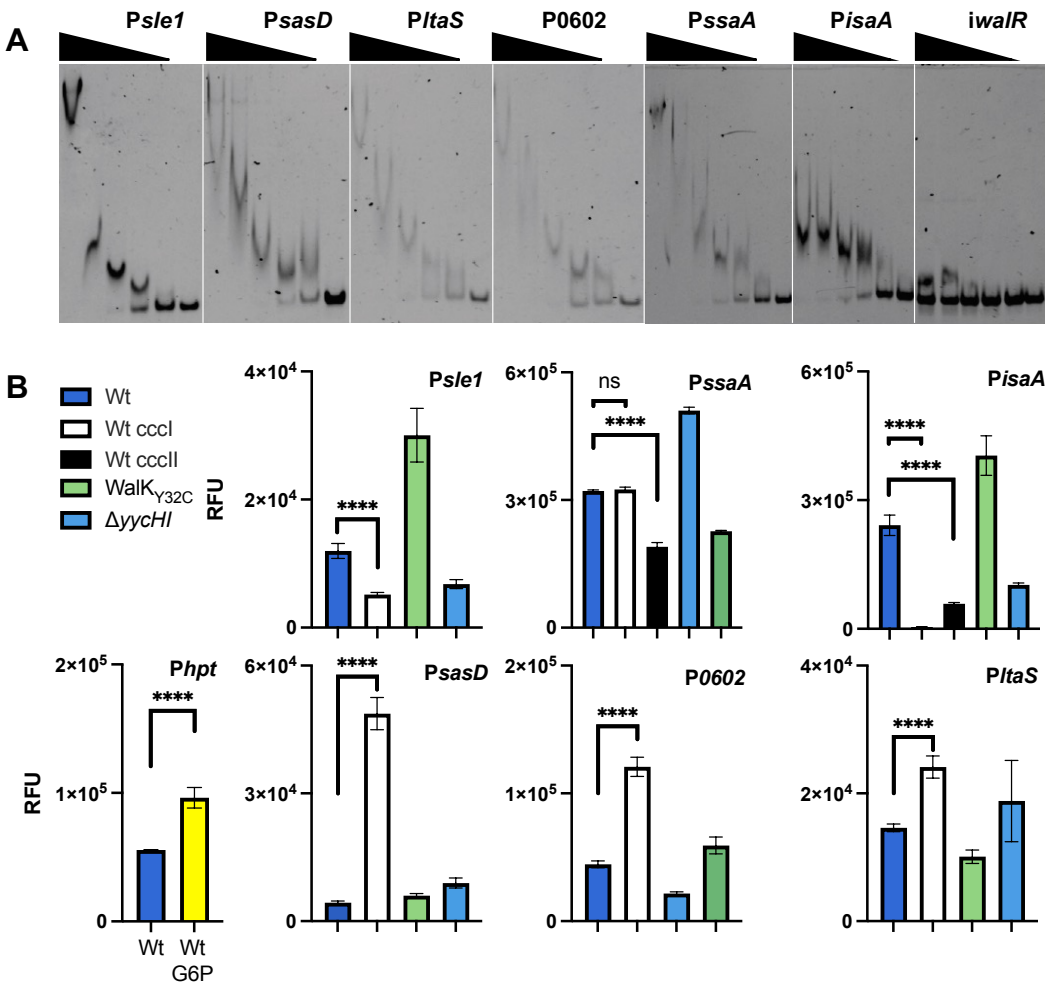

Figure 5. In vitro and in cellulo confirmation of WalR regulation. *A) Dose dependent band shifts caused through specific WalR binding to the ChIP-seq identified promoter regions. An intragenic region of the walR gene was used as a non-specific control (iwalR). A total of 5 doubling dilutions (plus a no protein control – right lane) of WalR starting at 20 µM, for all except PssaA where 40 µM was used. B) Cumulative YFP fluorescence of S. aureus reporter strains from stationary phase cultures. The glucose-6-phosphate (G6P) inducible hpt gene was used as a positive assay control through addition of 25 µM of G6P. Promoter activity was assessed in NRS384, with or without an abrogating (ccc) mutation in the WalR binding site. The native promoter construct was also analysed in WalK$_{Y32C}$ ('up' mutant) or ΔyycHI ('down' mutant) strains. Results are means from three independent experiments with the error bars showing the standard deviation of the mean. The significance of the ccc mutation was determined using an unpaired Student's t test; ns: not significant, <0.0001: **** versus the Wt promoter in NRS384.*

255

256 down regulated genes (*sasD*, *ltaS,* and SAUSA300_0602), exhibited increased fluorescence
257 upon abrogation of the WalR binding motif, showed increased fluorescence in the 'down'
258 mutant (Δ*yycHI*), and decreased fluorescence in the 'up' mutant ($WalK_{Y32C}$), indicative of
259 negative regulation by WalR [Figure 5B]. For upregulated genes, abrogation of the WalR
260 binding motif caused a reduction in fluorescence, with all showing increased activity in the
261 $WalK_{Y32C}$ background and decreased activity in the Δ*yycHI* mutant, characteristic of positive
262 WalR regulation [Figure 5B]. As the *isaA* and *ssaA* promoter regions contain two WalR binding
263 motifs, both were individually mutated. For *isaA*, the WalR binding site closest to the TSS
264 (CCCI, 37 bp to TSS) caused the greatest decrease in promoter activity [28], whereas for *ssaA*,
265 only the more distal binding site (CCCII, 167 bp from the TSS) reduced expression, which
266 corresponded to the single ChIP-seq peak for *ssaA* [Figure 4D].
267
268 **Control over additional essential genes by WalKR**
269 To investigate WalKR essentiality in *S. aureus* and triage genes for further analysis based on
270 their likely contribution to the essentiality phenotype, we analysed intersecting data sets
271 where genes fulfilled the following criteria: (i) contain a predicted upstream WalR-binding
272 site; (ii) belong to the core *S. aureus* genome; (iii) essential for growth in rich media [41, 42, 43];
273 and (iv) their expression is significantly changed upon WalK activation as defined by RNA-seq
274 [Figure 3A]. We found that within the predicted direct WalR regulon, seven essential genes
275 undergo a significant change in gene expression upon activation by WalKR (FDR $\leq$0.05, $\log_2$FC
276 $\geq$0.585) [Figure 3AB]. These genes were *ltaS* (see above); *dnaA*, which encodes chromosomal
277 replication initiator protein; *hup,* the sole DNA-binding protein HU; *prs*, which encodes a
278 ribose-phosphate pyrophosphokinase involved in purine salvage and de novo synthesis; *rplK,*
279 ribosomal protein L11 (50S subunit component); and *tagG* and *tarF*, which encode teichoic

acid biosynthetic proteins [Figure 6AB]. Additionally, three essential genes had a predicted upstream WalR binding site but did not undergo a significant change in expression: *dnaD*, *rnz*, and *sufB*, encoding putative replication restart protein DnaD, ribonuclease Z, and FeS assembly protein SufB. Of these three essential genes, a ChIP-seq peak was identified upstream of *dnaD* [Figure 6A].

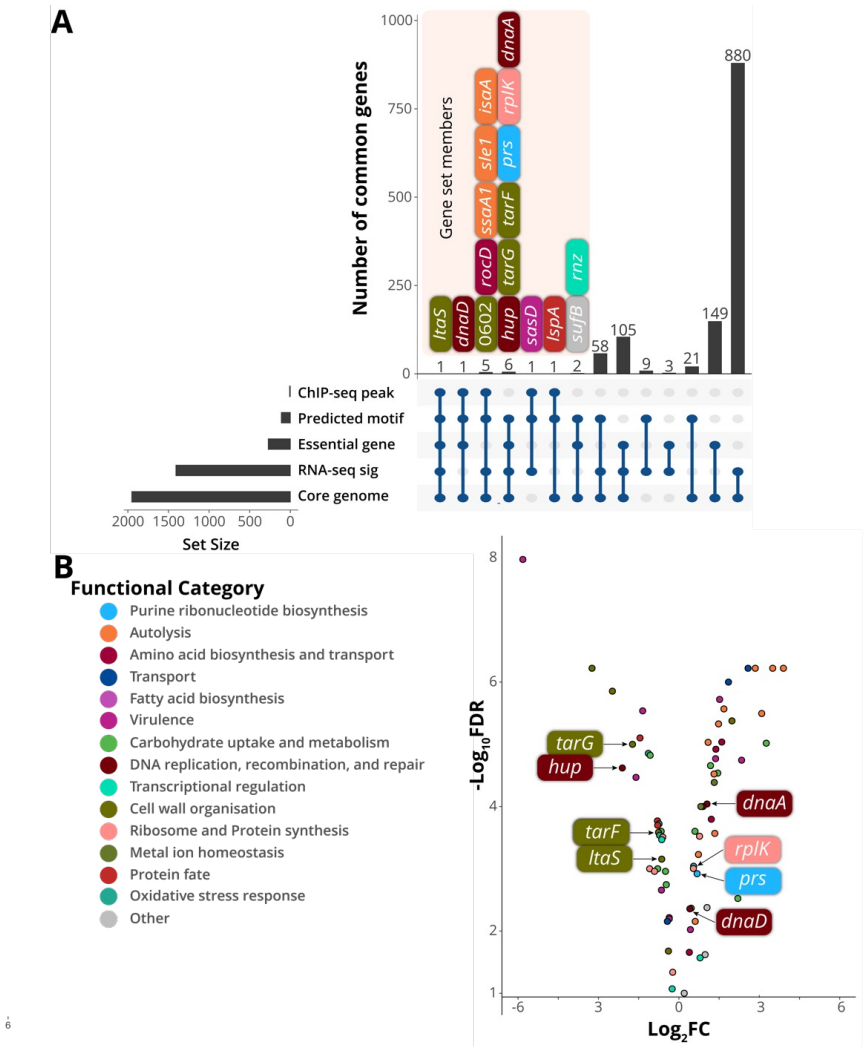

Figure 6. Analysis of putative WalR controlled essential genes. *A) Intersections between essentiality analysis and -omics data displayed as an UpSet plot. Members of gene sets where n<8 are shown. RNA-seq significance ((RNA-seq sig) FDR £0.05, log2FC ≥0.585). B) Gene expression changes of the predicted direct WalKR regulon upon WalK activation (Wt vs WalK$_{T389A}$). Essential genes with predicted WalR binding sites are highlighted.*

286 To further characterise the seven essential genes within the predicted direct WalR
287 regulon and *dnaD* [44, 45] [Table S3], we built a time-resolved picture of their expression. The
288 promoter regions for these genes, with or without an abrogating mutation (TGT to CCC) in the
289 WalR-binding site, were introduced into a luciferase reporter plasmid and transformed into
290 *S. aureus* NRS384 [Figure 7A-C]. The resulting *S. aureus* strains were monitored for growth
291 and light emission every 10 min over an 8 h period. For comparison, promoters from the
292 previously characterised WalR regulated genes and the *walR* gene itself were included [Figure

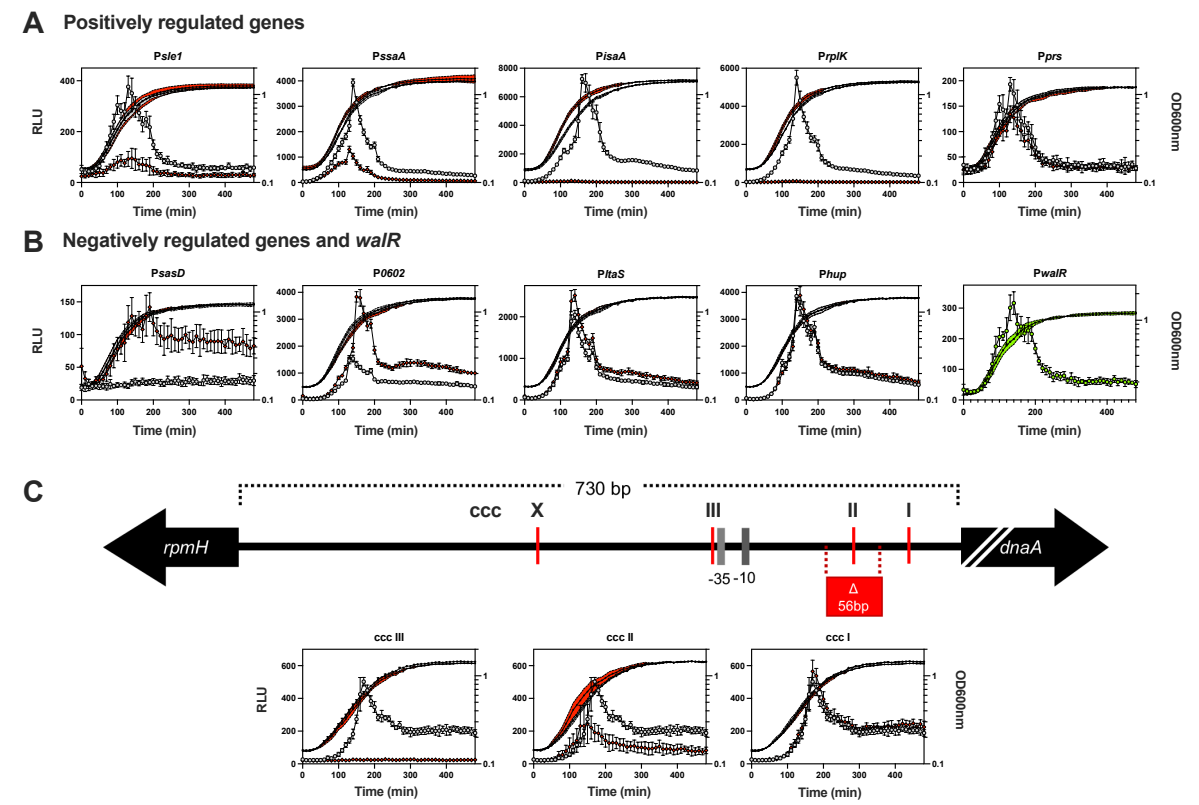

Figure 7: Characterising the temporal control of WalR on essential S. aureus genes. *A) Positively and B) negatively WalR regulated genes coupled to bacterial luciferase reporters showing the changes in promoter activity of the Wt (open grey circle: RLU; filled black circles: OD600nm) or the ccc (open red diamond: RLU; filled black diamond: OD600nm) mutated WalR binding site in LB media over time. Data represent the mean of three independent experiments (± standard deviation). Expression of walR is represented by green open circles (RLU), with growth indicated by filled black circles (OD600nm). C) Schematic (to scale, except dnaA – truncation indicated by white back slashes) of the dnaA promoter region with identified WalR sites denoted. The Wt and the three dnaA motif mutants (ccc I-III) were analysed as described above. Highlighted in red is the 56 bp deletion [47] and the -35 and -10 sites for the dnaA promoter.*

293 7AB]. Expression from the *walR* promoter rapidly peaked in mid-exponential phase and then
294 tapered off, as has been observed previously [Figure 7B] [46]. The previously ascribed WalR
295 regulation of the six ChIP-seq hits were corroborated by the luciferase reporter assays;
296 mutation of the WalR binding site yielded a significant reduction in the level of expression
297 throughout growth for the positively regulated genes (*sle1, ssaA* and *isaA*)[Figure 7A]. While
298 an increased level of expression was observed in the negatively regulated genes upon
299 mutation of the WalR binding site mutation (*sasD*, SAUSA300_0602 and *ltaS*)[Figure 7B]. Loss
300 of the WalR negative regulation was shown to relieve repression of *sasD,* while the impact on
301 SAUSA300_0602 was most pronounced into stationary phase of growth. Only a subtle
302 difference in expression was observed for *ltaS*; mutational abrogation of WalR binding
303 prevented "turning off" of gene expression, resulting in prolonged expression into stationary
304 phase [Figure 7B]. We then examined the impact on the additional essential genes identified
305 from the analysis of the direct regulon. No regulation was detected for *tagG, tarF* or *dnaD*
306 [Figure S8]. However, the very low level of *dnaD* and *tarF* promoter activity under the
307 conditions tested precluded a definitive determination. Whereas a strong positive regulation
308 was observed for *rplK. prs* was also shown to be positively regulated. *hup* was shown to be
309 weakly negatively regulated by WalR, which caused a reduction in the expression upon the
310 transition into stationary phase, similar to *ltaS*. For hup there was a bi-phasic change at 190
311 min present in the Wt strain, which was lost when the binding site was mutated [Figure 7B].
312 Closer inspection of the large (730 bp) upstream intergenic region between the
313 divergent *dnaA* and *rpmH* genes revealed an enrichment of potential WalR binding motifs
314 upstream of *dnaA* [Figure 6B]. The three sites proximal to the *dnaA* gene were chosen for
315 further analysis (site X was not investigated, [Figure 7C]). Sites ccc II and ccc III impacted the
316 expression of *dnaA* while no change in expression was observed for the mutation of ccc I

317 [Figure 7C]. We observed both a negative regulation for ccc II and a complete abrogation of
318 expression for ccc III, suggesting a complex fine tuning of *dnaA* expression afforded by WalR.
319 Recently, a suppressor mutant with a deletion in the *dnaA* promoter that reduced the level
320 of DnaA activity (initiation of DNA replication) was identified in a *S. aureus Δnoc* strain [47]. This
321 deletion removed a 56 bp region surrounding the WalR binding site denoted by ccc II [Figure
322 7C]. Here, in agreement with this previous observation, we identified the reduced expression
323 from the *dnaA* promoter upon abrogation of the ccc II WalR binding site.
324

325 **Modulation of WalKR activity alters *S. aureus* lipoteichoic acid structure**

326 Lipoteichoic acid (LTA) is an anionic polymer composed of a repeating chain of glycerol
327 phosphate units anchored to the cell membrane via a diacylglycerol group and decorated with
328 side chain modifications of D-alanine and/or glycosyl moieties [48]. Here, the physiological
329 impact of negative *ltaS* regulation by WalR was assessed by extracting LTA from strains of
330 representing a spectrum of WalKR activities. Polyacrylamide gel electrophoresis (PAGE) of LTA
331 enables visualisation via laddered banding patterns, with each subsequent band representing
332 a polymer chain length of n + 1 [49]. Side chain modifications can also be observed, with high
333 levels of heterogenous modification resulting in loss of single band resolution, i.e., smearing
334 [49]. In the Wt or a 'down' mutant yielded a characteristic smeared banding pattern, indicative
335 of heterogenous side-chain modification, whereas in a WalKR 'up' mutant ($WalK_{T389A}$) LTA
336 chain length changes were observed. This manifested as a reduction in mid-length LTA [Figure
337 8, orange line] and increase in high molecular weight LTA [Figure 8, black line]. Analysis of the

338 supernatant of the 'up' strain resulted in LTA shedding, consistent with the compromised cell

339 wall [Figure 1C].

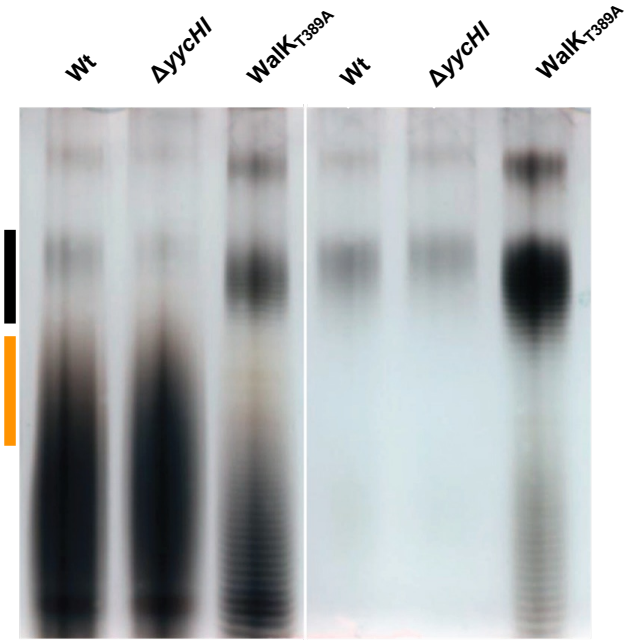

Figure 8. Assessing the influence of WalKR activity on LTA production. *PAGE analysis of purified LTA from NRS384 and isogenic mutant derivative strains grown in LB. Each band indicates a glycerol phosphate polymer length of n+1. Where bands are not clearly visible, this is due to heterogenous side chain modifications resulting in smearing patterns. Black and orange lines are shown and represent regions of distinct difference in LTA banding patterns between the strains.*

340 **WalR controls DNA compaction by regulation of the DNA binding protein HU**

341 The essential gene *hup* [50], encodes the sole *S. aureus* DNA-binding protein HU, was indicated

342 to be negatively regulated by WalR [Figure 7B]. *S. aureus* HU belongs to a family of low

343 molecular weight nucleoid-associated proteins (NAPs) and although it is largely

344 uncharacterised, its structure has been determined [51]. Orthologs of HU NAPs from other

345 bacteria have previously been shown to control DNA compaction, introducing negative

346 supercoils into relaxed DNA [52, 53], and play an essential role in the initiation of DNA replication

347 in *B. subtilis* [54]. To investigate potential changes in DNA topology mediated by *S. aureus* HU

348 and WalR regulation of HU, we performed CRISPRi knockdown of *walR, hup,* and as a negative

349 control, *hla*. The CRISPRi knockdown titrated the expression of each targeted gene [Figure

350

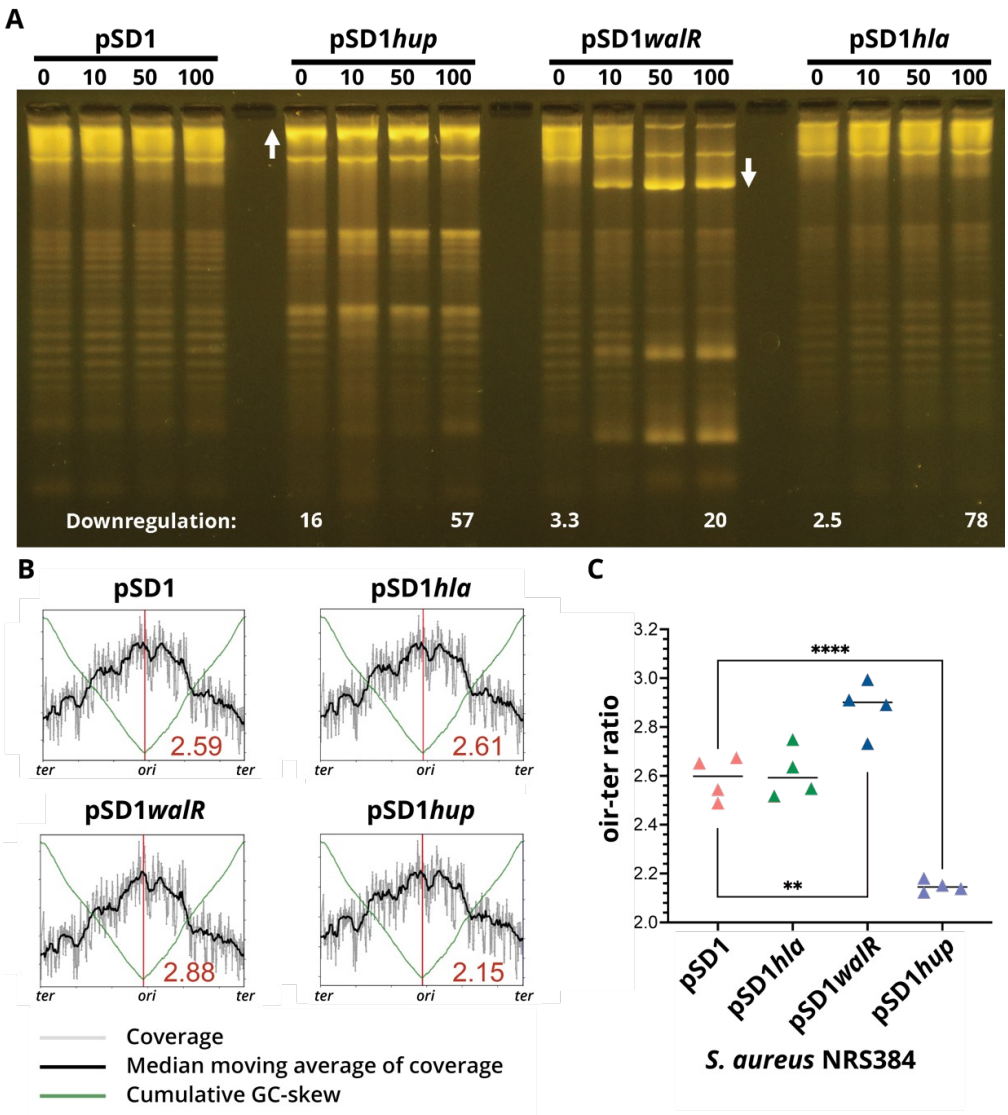

Figure 9. Impact of CRISPRi mediated downregulation of hup or walR on DNA topology. *A) NRS384 containing either pSD1 (empty vector), pSD1hup, pSD1walR or the negative control pSD1hla were induced with increasing concentrations of aTc (0, 10, 50 and 100 ng/mL). At 5 h post induction total RNA and plasmids were isolated. Plasmids were run on a 1% (w/v) TBE gel containing 2.5 µg/mL chloroquine to allow for the resolution and visualisation of discrete topoisomers of supercoiled plasmid DNA. Relative fold downregulation of each targeted gene compared to uninduced vector control (pSD1, 0) as determined by RT-qPCR is denoted at the bottom of the image. The image is representative of three repeat experiments. B) A representative whole genome sequencing read-coverage graph showing the ori-ter ratios for the four CRISPRi constructs under 100 ng/mL aTc induction. Each plot represents one of four biological sequencing replicates for each CRISPRi construct. Shown in the bottom right quadrant of each graph is the mean ori-ter ratio across the four replicates. The ori-ter ratio between the sequence read coverage at the origin and terminus. C) Summary graph of ori-ter ratios for each of the four CRISPRi constructs induced with 100 ng/mL of aTc to downregulate expression of the three targeted genes (hla, walR and hup). Shown are the mean of quadruplicate, independent biological replicate sequencing experiments. Differences between means assessed using an unpaired student's t test, **p=0.0059, ***p=<0.0001.*

351 9A], resulting in 57-, 20-, and 78-fold downregulation of *hup*, *walR*, and *hla*, respectively.
352 Notably, a degree of knockdown in the absence of inducer was observed, attributable to the
353 leaky expression of the CRISPRi guide and the location of the guide (overlapping the promoter
354 for *hup*). HU knockdown resulted in a relaxation of plasmid supercoiling, shown by increased
355 DNA band intensity during chloroquine gel electrophoresis, due to more slowly migrating
356 topoisomers in comparison to the control [Figure 9A pSD1 vs pSD1*hup*, white up arrow].
357 Knockdown of *walR* had the opposite effect, indicated by increased DNA band intensities
358 arising from faster migrating topoisomers with greater supercoiling density [Figure 9A pSD1
359 vs pSD1*walR*, white down arrow]. This observation is consistent with a model where WalR
360 negatively regulates HU and is further supported by the knockdown of *hla* or the empty vector
361 having no impact on DNA topology [Figure 9A pSD1 vs pSD1*hla*]. These results show that *S.*
362 *aureus* HU, as observed in other bacteria, increases the supercoiling density of DNA. We
363 propose that the negative regulation of *hup* by WalR has the opposite effect, causing the
364 relaxation of supercoiling and leading to decreased compaction of cellular DNA.
365
366 **Changes in initiation of DNA replication mediated by WalR and HU**
367 We next assessed whether WalKR modulation of *hup* could also impact the initiation of DNA
368 replication in *S. aureus*, building on the observation that this was impaired in *B. subtilis* by
369 depletion of orthologous protein [55]. This was addressed by genome sequencing of the CRISPRi
370 knockdown constructs of *S. aureus* for *walR, hup, hla* and vector control, and aTc induction (0
371 or 100 ng/mL^{-1}) and determining the number of chromosome replication origins per cell
372 during exponential growth [47, 54]. Mean *ori*-to-*ter* ratios were calculated and revealed a
373 significant reduction in the *ori*-to-*ter* ratio from ~2.60 in the vector control and non-target *hla*
374 control compared to 2.15 when the expression of *hup* was repressed [Figure 9BC]. A

375 significant increase (2.88) in the mean *ori*-to-*ter* ratio, was observed when *walR* was
376 repressed [Figure 9BC], consistent with the negative regulation of *hup* by WalR [Figure 7B].
377 Taken together, these data show that *S. aureus* HU contributes to promoting initiation of DNA
378 replication and is directly influenced by WalKR-mediated regulation.

379 Collectively, our findings above link diverse and crucial cellular processes, including
380 DNA replication and cell wall homeostasis, to the activity of WalKR. Distinct from other
381 bacilliota, WalKR appears to serve as a crucial nexus for both regulatory and temporal
382 coordination of these diverse activities. Thus, this work provides a mechanistic basis for the
383 essentiality of WalKR in *S. aureus*.

384

385 **Discussion**

386 Here we use ChIP-seq to define genes directly under the control of WalKR. Subsequently, we
387 generated a *S. aureus* specific WalR consensus binding motif and to inform physiologically
388 relevant cut-offs for interrogating transcriptomic data obtained when mutationally activating
389 WalK. These experiments allowed us to define a direct and indirect WalKR regulon. These
390 results confirm and expand the pioneering discoveries of Dubrac and Msadek *et al*., with
391 WalKR directly regulating several autolysins with activation increasing the production SaeRS
392 regulated virulence genes [7, 12, 24]. Additionally, consistent with our earlier work [56], we
393 observed upregulation of a variety of genes involved in central metabolism upon WalK
394 activation, particularly those involved in amino acid, purine, and fatty acid biosynthesis.
395 Filtering our results on essential genes directly controlled by WalKR, we identified and defined
396 new members of the WalKR direct regulon; *rplK*, *hup, ltaS, prs* and *dnaA*. Of which, *prs* and
397 *rplK*, belong to the central metabolic pathways of purine and protein biosynthesis,
398 respectively.

399 We find that WalKR negatively regulates the expression of *ltaS,* dampening expression
400 from late exponential into stationary phase. To our knowledge, this is the first report of direct
401 transcriptional regulation of *ltaS*, although post-translational regulation has been described
402 [57]. We also detected VraR binding to a second site further upstream in the *ltaS* promoter.
403 Though comparative transcriptomics *ltaS* (N315 locus tag SA0674) has previously been
404 mapped to the VraSR regulon as a positive regulator [58], however, direct control was not
405 demonstrated [38]. It is not surprising that WalKR and VraSR regulate *ltaS* transcription as both
406 TCSs are intimately connected to cell wall homeostasis. WalKR maintains a balance of
407 peptidoglycan cleavage that allows the cell to grow but not lyse [10, 18], and VraSR governing

408 the cell wall stress stimulon in response to extracellular insult [59, 60]. Together, LTA and wall
409 teichoic acid are present in the Gram-positive cell wall in roughly equal proportion to
410 peptidoglycan [61]. Modulation of *ltaS* expression by two TCSs that integrate different signals,
411 alongside post-translational regulation of the enzyme, presumably ensures tight and finely
412 tuned control of *ltaS* activity, enabling co-ordination of LTA synthesis with peptidoglycan
413 remodelling. Upon WalK activation, we observed a change in LTA chain length and reduction
414 in modification. As LTA chain length is an intrinsic property of the LtaS enzyme that is dictated
415 by the availability of lipid starter units [62], it is unlikely that the chain length differences
416 observed upon activation of WalK are solely attributable to direct negative regulation of *ltaS*.
417 We speculate that the global transcriptional rewiring of the cell upon WalK activation may
418 affect the availability of lipid starter units, although this remains to be investigated.

419 In addition to its role in teichoic acid biosynthesis, we found that WalKR controls
420 essential genes involved in the initiation of DNA replication. In *S. aureus*, DNA replication is
421 initiated by binding of DnaA to AT-rich regions at the origin of replication, *oriC* [63]. This process
422 is tightly controlled, as mistiming of initiation results in aberrant cell division [64]. We show that
423 WalKR can both positively regulate the expression of *dnaA* and negatively regulate *hup.* The
424 role of *hup* in staphylococcal DNA replication initiation has not previously been investigated
425 but recently in *B. subtilis* the *hup* homologue *hbs* has been shown to promote initiation [65]. We
426 show this function is conserved in *S. aureus*; knocking down expression of *hup* resulted in
427 reduced initiation of DNA replication. In addition to *hup,* two other regulators of DNA
428 replication initiation have been characterised in *S. aureus*; Noc and CcrZ [64]. Noc is a negative
429 regulator of DnaA driven initiation [47], whereas CcrZ is a positive regulator [64]. The mechanisms
430 underlying the control of DnaA by these proteins are yet to be fully defined, however it is
431 unlikely that Noc directly regulates *dnaA* expression [47] and CcrZ may act post-translationally,

432 by phosphorylating an unknown intermediate factor [64]. A recent investigation into the role of
433 Noc in *S. aureus*, a suppressor mutant down regulating the activity of DnaA was identified
434 with a deletion of a 56bp region [Figure 7C] within the 5'UTR of *dnaA* [47]. We show this function
435 is conserved in *S. aureus*; knocking down expression of *hup* resulted in reduced initiation of
436 DNA replication. In addition to *hup,* two other regulators of DNA replication initiation have
437 been characterised in *S. aureus*; Noc and CcrZ [64]. Noc is a negative regulator of DnaA driven
438 initiation [47], whereas CcrZ is a positive regulator [64]. The mechanisms underlying the control of
439 DnaA by these proteins are yet to be fully defined, however it is unlikely that Noc directly
440 regulates *dnaA* expression [47] and CcrZ may act post-translationally, by phosphorylating an
441 unknown intermediate factor [64]. In a recent investigation into the role of Noc in *S. aureus*, a
442 suppressor mutant down regulating the activity of DnaA was identified with a deletion of a
443 56bp region [Figure 7C] within the 5'UTR of *dnaA* [47]. As this region encompasses one of two
444 characterised WalR binding motifs upstream of the gene, we propose that the loss of positive
445 WalR control through deletion of the binding site explains the observed decease in DnaA
446 activity. Additionally, RNA-seq showed an overall increase in *dnaA* expression (1.05 Log_2FC -
447 $WalK_{T389A}$ vs Wt) in exponential phase upon WalK activation, further highlighting the positive
448 role WalR has on *dnaA* expression.

449 That WalR was found to positively regulate *dnaA* and negatively regulate *hup*, both of
450 which are promoters of initiation, is somewhat counterintuitive. Knockdown of *walR*
451 expression caused over-initiation, consistent with its negative control of *hup* but
452 contradictory to its positive regulation of *dnaA* [Figure 8BC]. It may be that loss of HU is a
453 dominant phenotype, reducing initiation even in the presence of higher levels of DnaA, or
454 alternatively, that regulation of each gene is temporally distinct. The latter hypothesis is
455 supported by our observation that *dnaA* regulation occurred during exponential phase

456 whereas regulation of *hup* was in stationary phase [Figure 7C]. However, exactly how WalKR
457 transcriptional regulation of both *dnaA* and *hup* works in concert with post-translational
458 control mediated by HU, Noc and CcrZ to ensure tight, spatiotemporally accurate, control of
459 initiation of DNA replication remains to be elucidated. It is of note that during the discovery
460 of WalR in *B. subtilis* using a temperature-sensitive mutant, anucleate cells were observed at
461 the non-permissive temperature. This observation hints at the possibility of a wider
462 association between WalR and DNA replication in other Bacillota [9].

463 HU is a multifunctional protein, in addition to its role in DNA replication initiation, it
464 also contributes to DNA compaction, introduces negative supercoils into DNA [52] and can
465 impact localised gene regulation [66]. As we observed opposite changes to DNA supercoiling
466 caused by depletion of *walR* and *hup*, we propose that the negative regulation of HU by WalR
467 causes relaxation of supercoiling and may lead to decreased compaction of cellular DNA.
468 Transcriptional regulation of *hup* expression has not previously been described in *S. aureus*.
469 However, qualitative western blots have shown HU to be continuously present in the
470 staphylococcal nucleoid throughout all growth phases [67]. Taking this into account, we propose
471 that WalKR regulation of *hup* is not a binary switch, but rather provides tuneable control of
472 this essential system. Intriguingly, in *Mycobacterium tuberculosis* the serine/threonine kinase
473 PknB negatively regulates HU DNA binding through phosphorylation [68] and in *S. aureus*, PknB
474 mediated phosphorylation activates WalR [69]. Furthermore, a PknB phosphorylation site on
475 HU has been experimentally identified in *S. aureus* [70]. Therefore, PknB may directly repress
476 HU DNA binding through post-translational modification and indirectly represses the
477 expression of *hup* through activation of WalR.

478 The reason for essentiality of WalKR differs across Bacillota species [71]. In *S. aureus,*
479 essentiality is proposed to result from polygenic control of non-essential autolysins involved
480 in the cleavage and relaxation of peptidoglycan crosslinks, allowing expansion of the cell wall
481 [6]. Here, we extend this hypothesis, showing WalKR direct control of at least five essential
482 genes (*rplK*, *hup, ltaS, prs* and *dnaA*) not directly involved in peptidoglycan biosynthesis but
483 intimately linked with cell growth and cell division. Thus, we propose that WalKR essentiality
484 arises though polygenic co-ordination of multiple cellular processes; ribosome assembly,
485 peptidoglycan homeostasis, LTA polymerisation, DNA topology, and the initiation of DNA
486 replication, ultimately making WalKR an indispensable link between cell wall homeostasis and
487 DNA replication. We propose a model in which WalK senses a currently unknown ligand
488 during logarithmic growth through the extra-cytoplasmic PAS domain, resulting in
489 autophosphorylation, dimerisation, and maximal interaction between WalK and WalR [Figure
490 10A]. The level of WalK activation can also be dynamically tuned in response to the metalation
491 state of the intracellular PAS domain [28]. WalK:WalR interaction allows phosphotransfer to
492 WalR residue D53, whilst a second WalR site T101 can be phosphorylated through the PknB
493 kinase (recognises muropeptide fragments[72]). Phosphorylated WalR binds the cognate
494 recognition motifs of its direct regulon as a dimer, causing either negative or positive changes
495 to gene expression, primarily dependent on the position of the binding motif in relation to
496 the transcriptional start site [Figure 10B]. The direct WalR regulon has three broad functions;
497 i) control of cell wall metabolism through regulation of a suite of autolysins governing
498 peptidoglycan homeostasis and fine tuning of LTA biosynthesis through negative regulation
499 of lipoteichoic acid synthase; ii) linking initiation of DNA replication to cell wall homeostasis
500 through regulation of *dnaA* and *hup*; iii) signal amplification through modulation of
501 transcription factors, selected other TCSs, and via negative regulation of DNA binding protein

502 HU [Figure 7B]. Together with the downstream effects of changes in cell wall metabolism,

503 signal amplification drives changes in expression of the indirect WalKR regulon, producing a

504 large shift in cellular transcription that includes the increased expression of virulence factors

505 and metabolic genes [Figure 10C].

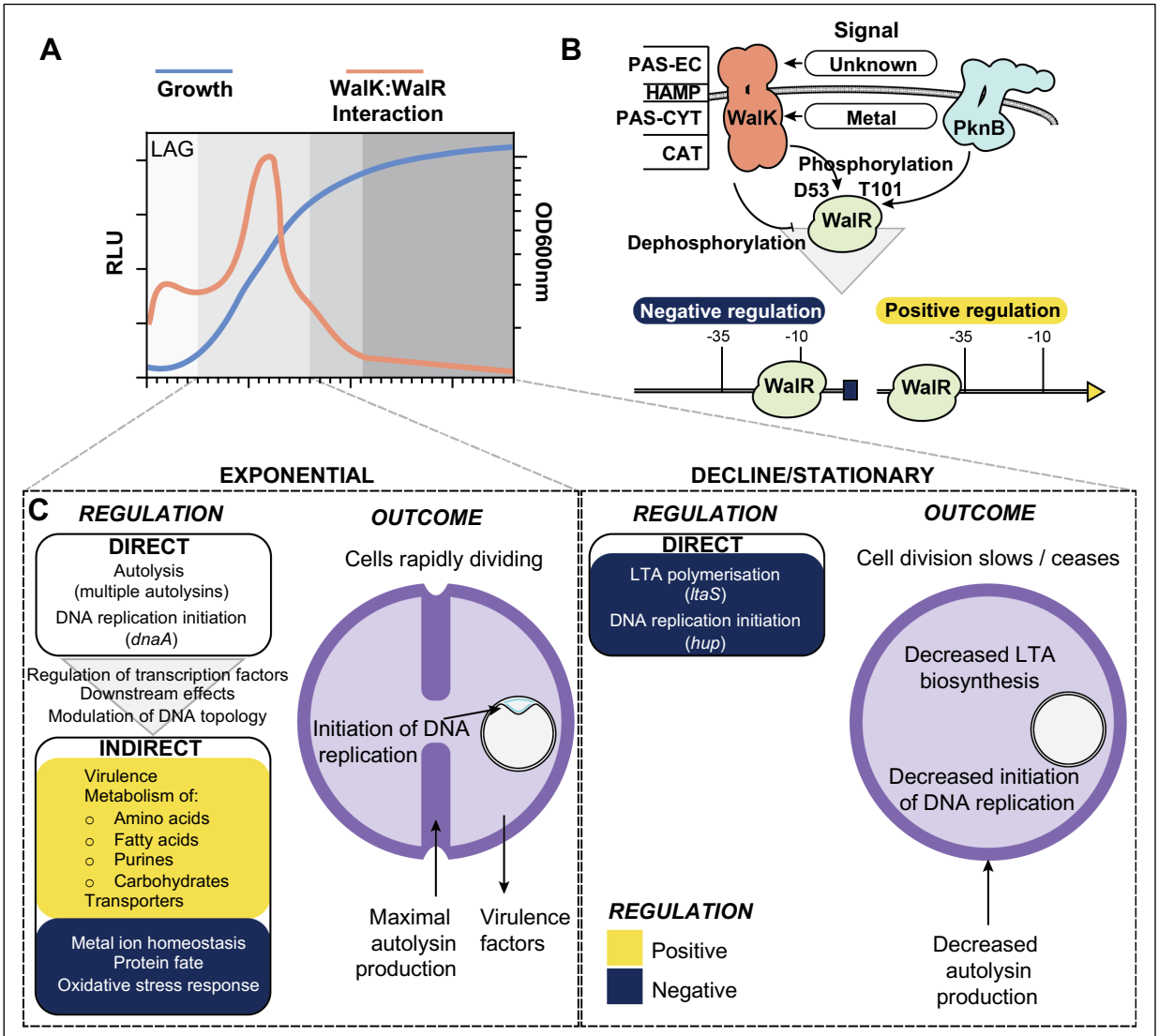

Figure 10. A model of the role of WalKR in cell division. *A) Changes in the interaction of WalK with WalR throughout growth. B) Mechanism of signal transduction and transcriptional control of WalKR. -35 and -10 denote promoter regions. PAS-EC: Per-Arnt-Sim extracellular, HAMP: present in Histidine kinases, PAS-CYT: PAS-cytoplasmic, CAT: catalytic domain. C) Transcriptional changes and their outcomes for the direct and indirect WalKR regulon during different growth phases. Yellow and dark blue denote positively, and negatively, regulated gene sets, respectively.*

506 WalKR has long been considered a promising target for the development of novel anti-

507 Gram-positive agents [73], although to date no WalKR targeted compounds have been

508 successfully developed. Despite this, the system remains a viable target for conventional
509 antibacterial chemotherapy due to its role as a signal integrating nexus of essential cellular
510 functions and the presence of two PAS domains capable of binding small molecules inside and
511 outside of the cell [18, 28]. Increasingly, alternative strategies to traditional antibacterial
512 chemotherapy are being explored, including the development of so called "antibiotic
513 resistance breaking (ARB) compounds" that re-sensitise resistant strains to existing antibiotics
514 [74, 75]. Here, we found that mutationally activated WalKR 'up' mutants were more sensitive to
515 three different antibiotic classes targeting the cell wall: oxacillin, tunicamycin, and
516 vancomycin. In contrast, recent work conducted using the methicillin sensitive *S. aureus*
517 (MSSA) strain ATCC29213 found the opposite; a WalKR 'down' mutation ($WalR_{T101M}$)
518 increased tunicamycin sensitivity [76]. Tunicamycin is a dual targeted antibiotic, binding to MraY
519 and TarO, which belong to the peptidoglycan recycling and wall teichoic acid synthesis
520 pathways, respectively [77]. In MSSA ATCC29213, decreased WalKR activity results in indirect
521 downregulation of enzymes within the peptidoglycan recycling *mupG* operon, as well as direct
522 downregulation of autolysins. Together these gene expression changes starve MraY of
523 precursor molecules, making the enzyme exquisitely sensitive to tunicamycin [76]. In MRSA
524 NRS384 the genes of the *mupG* operon were not differentially regulated upon WalKR
525 activation. Consequently, we conclude that tunicamycin sensitivity in NRS384 'up' mutants
526 likely arises through a different mechanism. More broadly, differences in the indirect WalR
527 regulon between MRSA and MSSA may reflect regulatory adaptions necessary to
528 accommodate the exogenous, *mecA* encoded, PBP2a transpeptidase into the complex
529 process of cell wall homeostasis [78]. Here, we found that mutational stimulation of normal
530 WalKR activity rendered NRS384 MRSA susceptible to oxacillin despite the presence of *mecA*,

531 opening an alternative avenue for future WalKR focused drug development; the discovery of

532 ARB compounds that phenocopy WalKR activating mutations.

533

534 ## Materials and Methods

535 **Strains, oligonucleotides, media, and reagents**

536 Bacterial strains and plasmids are listed in Table S5. Oligonucleotides (IDT) used in this study
537 are listed in Table S6. *Escherichia coli* were routinely cultured in LB (Merck) or on L-agar (1.5%
538 [w/v] agar added) unless stated otherwise. *S. aureus* were routinely grown on Brian Heart
539 Infusion (BHI) agar (Bacto, BD Biosciences) or Sheep blood agar. When cultured in broth, they
540 were grown in Brain heart infusion broth Trypticase soy broth (TSB, Oxoid), or LB with shaking
541 at 200 rpm. For selection, antibiotics (Sigma) were added at the following concentrations for
542 *E. coli* (*E.c*) and *S. aureus* (*S.a.*): Ampicillin 100 µg/mL^{-1} – *E.c.*, Kanamycin 50 µg/mL^{-1} – *E.c.*/*S.a.*,
543 Chloramphenicol 10 µg/mL^{-1} – *E.c.*/*S.a*. Restriction enzymes, Phusion DNA polymerase, and T4
544 ligase were purchased from New England Biolabs. Phire Hotstart II DNA polymerase for colony
545 PCR was purchased from Thermo Fisher.

546

547 ***S. aureus* site-directed mutagenesis by allelic exchange**

548 Upstream and downstream regions of the point mutation for *walK*^{T389A}
549 (IM7/IM120/IM121/IM10), *walR*^{T101A} (IM31/IM232/IM233/IM10) or *spa* deletion
550 (IMT275/IMT353/IMT354/IMT278) were PCR amplified and then a SOE-PCR was performed
551 on the gel extracted template to generate an amplicon for SLiCE cloning into pIMAY-Z [79]. This
552 yielded plasmids pIMAY-Z *walK*^{T389A}, pIMAY-Z *walR*^{T101A} and pIMAY-Z Δ*spa*. To construct
553 pIMAY-Z *walK*^{Y32C}, genomic DNA from a sectored mutant of NRS384 Δ*yycHI* (containing an
554 additional *walK*^{Y32C} mutation) was amplified with primers IM107/IM10 and the amplicon
555 cloned as described above. Construction of isogenic mutants of NRS384 by allelic exchange
556 was performed as described previously [79]. The WalK enhancing mutations could visually be

557 discriminated from the wild type due to reduced colony size and opacity. For the WalR^{T101A},
558 the mutation was screened by colony PCR (70°C annealing temperature) with primers
559 IM233/IM181. From putative mutants, genomic DNA was extracted from 1 ml of overnight
560 culture (DNeasy Blood and Tissue Kit—Qiagen) pre-treated with 100 µg of lysostaphin (Sigma
561 cat. no. L7386) and sequenced on an Illumina NextSeq by the Doherty Applied Microbial
562 Genomics facility (University of Melbourne). Resultant reads were mapped to a NRS384
563 reference genome [80] and mutations identified using Snippy
564 (https://github.com/tseemann/snippy).

565

566 **Construction of pRAB11-FLAG**

567 To construct a vector for the C-terminal FLAG tagging of *S. aureus* proteins, the
568 anhydrotetracycline inducible vector pRAB11 [34] was digested with KpnI to linearise and gel
569 extracted. The 6.4kb vector was then amplified with primers IM512/IM513 to add in a
570 consensus ribosome binding site (IM512), a 1xFLAG tag and downstream *tonB* transcriptional
571 terminator (IM513). The amplimer was digested with KpnI, gel extracted, re-ligated to yield
572 pRAB11-FT. The sequence of the plasmid was verified by sequencing on the Illumina platform.
573 To clone into pRAB11-FT, the vector was digested with KpnI, gel extracted and used as
574 template with primers IM514/IM515 to amplify the vector backbone. Response regulators
575 (WalR - IM516/IM517), (SaeR - IM518/IM519), (VraR - IM520/IM521), (HptR - IM522/IM523)
576 were amplified from the start codon and omitting the stop codon with NRS384 genomic DNA.
577 The products were gel extracted, SLiCE cloned into amplified pRAB11-FT and transformed into
578 IM08B, yielding pRAB11:*walR*^{FLAG}, pRAB11:*saeR*^{FLAG}, pRAB11:*vraR*^{FLAG} and pRAB11:*hptR*^{FLAG}.
579 The plasmids were electroporated into NRS384Δ*spa*.

580

581 **Construction of pIMC8-YFP reporter strains and assay for YFP activity.**

582 Promoter regions for *sasD* (IM1127/IM1107), *sle1* (IM1108/IM1109), *P602* (IM1129/IM1110),
583 *ltaS* (IM1111/IM1112), *ssaA* (IM1130/IM366) *isaA* (IM1128/IM364 were PCR amplified from
584 NRS384 genomic DNA and gel extracted. The vector pIMC8-YFP [28] was digested with KpnI, gel
585 extracted and PCR amplified with IM1/IM385. The amplified promoters and vector were SLiCE
586 cloned, transformed into IM08B and subsequently electroporated into NRS384, NRS384
587 Δ*yycHI* or NRS384 *walK*^{Y32C}. Mutations disrupting the WalR motif (1st TGT to CCC) were
588 introduced by SOE-PCR with the bracketed primers sets for *hpt* (IMT300/IMT301); *sle1*
589 (IM1108/IM1115; IM1114/1109), *P0602* (IM1129/1119; IM1118/IM1110), *ltaS*
590 (IM1111/IM1117; IM1116/IM1112), *ssaA*^{CCCI} (LS371/LS376; LS375/LS372), *ssaA*^{CCCII}
591 (LS371/IM1121; IM1120/LS372), *isaA*^{CCCI} (IM1128/IM1123; IM1122/IM364), *isaA*^{CCCII}
592 (IM1128/IM1125; IM1124/IM364). The resultant mutated promoters were gel extracted,
593 SLiCE cloned, transformed into IM08B and subsequently electroporated into NRS384. For the
594 *sasD* promoter the mutation was incorporated into the reverse primer (IM1113) in
595 combination with IM1127. To assess YFP production, each strain was grown in 5 ml of LB
596 containing 10 µg/mL^{-1} chloramphenicol in a 50 ml tube for overnight at 37°C with shaking at
597 200 rpm. The culture was diluted 1:100 in 5 ml of fresh LB containing chloramphenicol and
598 incubated overnight. The fluorescence (excitation 512 nm, emission 527 nm) of each strain
599 (200 µl – Nunc black well plates) was read in triplicate using an Ensight multimode plate
600 reader (PerkinElmer) set to 100 flashes per well. Resultant data was plotted using the
601 GraphPad Prism (v9.3.1) software package.

602

603 **Production and purification of proteins.**

604 For production of WalR, Rosetta 2 (DE3) pET28(a):*walR* was grown in 2 L of autoinduction
605 media [81] at 25°C for four days with vigorous shaking, and cells were harvested by
606 centrifugation. For production of VraR Rosetta 2 (DE3) pET21(d): *vraR* was grown in 2 L of LB
607 at 37°C with vigorous shaking to an OD600 nm of 0.6, chilled on ice for 10 min then induced
608 with 1 mM IPTG. Subsequently, cells were grown for a further 16-20 h at 18 °C with vigorous
609 shaking and harvested by centrifugation. For purification of both proteins, cell pellets were
610 resuspended at 3 ml/g in buffer A (50 mM NaH_2PO_4 [pH 8.0]) with 300 mM NaCl and 10 mM
611 imidazole. To enhance lysis and prevent proteolysis, 7000 U chicken egg-white lysozyme
612 (Sigma), two complete EDTA-free protease inhibitor tablets (Roche) and 20 U DNase I (NEB)
613 were added. Cells were lysed by sonication and lysates were clarified by centrifugation at
614 30,000 x *g* for 30 minutes at 4°C. The cleared lysate was loaded onto a 25 mL free-flow gravity
615 column (GeneFlow) packed with 3 ml TALON® Metal Affinity Resin (Takara Bio), washed with
616 10 column volumes (CV) of buffer A containing 20 mM imidazole and 2 M NaCl. The protein
617 was eluted in 2 CV of buffer A containing 150 mM imidazole and 300 mM NaCl and dialysed
618 overnight 6 kDa MWCO, CelluSep) into storage buffer (25 mM Tris [pH 8.0], 300 mM NaCl,
619 20 mM KCl, 10 mM $MgCl_2$, 1 mM DTT, 5% glycerol). The proteins were spin concentrated to 5
620 mg / ml (3 kDa MWCO, vivaspin 20, Sartorius), aliquoted, snap frozen in liquid nitrogen, and
621 stored at -80°C until required.

622

623 **Electrophoretic mobility shift assays (EMSAs)**

624 DNA duplex probes for electrophoretic mobility shift assay binding assays were generated by
625 annealing two 70 bp single-stranded oligonucleotides, one of which was labelled with Cy5

626 fluorophore on the 5' end (Table S6). Annealing was performed in duplex buffer (30 mM
627 HEPES [pH 7.5], 100 mM potassium acetate) by heating equimolar concentrations of
628 complimentary single-stranded oligonucleotide at 94°C for two min and then cooling to room
629 temperature over 30 min. Duplexes were subsequently gel-extracted from a 2% (w/v) agarose
630 1xTBE gel. Binding reactions were performed in a final volume of 25 µl of binding buffer
631 (25 mM Tris [pH 8.0], 300 mM NaCl, 20 mM KCl, 10 mM $MgCl_2$, 1 mM DTT, 4 µg BSA, 0.5 µg
632 salmon sperm DNA). Initially, varying concentrations of WalR/VraR were incubated for 5 min
633 at 25°C in binding buffer, then DNA probe was added to a final concentration of 16 nM and
634 the reaction was incubated for a further 15 min. After incubation, reactions were mixed (5:1)
635 with 6x Orange G loading buffer [82] and 5 µl was electrophoresed on an 8% polyacrylamide
636 native gel (29:1 acrylamide:bisacrylamide ratio) in 1xTBE at 4 °C. Bands were visualised using
637 a GE Amersham 600 imager in the Cy5 channel with a 10 min exposure time.

638

639 **Total RNA extraction and rRNA depletion**

640 A 10 ml LB (50 ml tube) culture was grown overnight at 37°C with shaking at 200rpm. The
641 saturated culture was diluted 1:100 into fresh 10 ml TSB and grown to an OD600nm of 0.8-
642 1.0. A 5 ml aliquot of culture was removed and added to 10 ml of RNAprotect Bacteria Reagent
643 (Qiagen) and mixed by vortexing. The sample was incubated at room temperature for 5 min.
644 Cells were then harvested by centrifugation (7,000*xg*/5min/22°C), the supernatant discarded
645 and the cell pellet resuspended in 1 ml of TRIzol (Invitrogen). Cells were lysed by bead beating
646 (Precellys 24 instrument - 6000 rpm, 1 min, 100 µm zirconium beads) and cell lysates were
647 clarified by centrifugation (20,000*xg*/10 min/4°C). Subsequently, 700 µl of supernatant was
648 removed and mixed with 700 µl of ethanol. RNA was extracted using a Direct-Zol RNA

649 miniprep plus kit (ZymoResearch) according to manufactures instructions, including the on-
650 column DNase I treatment step. Following RNA extraction, an additional DNA removal step
651 was performed using a TURBO DNA-free kit (Invitrogen) according to manufacturer's
652 instructions. The absence of DNA was accessed *by gyrB* PCR (IM1020/IM1021) on 1µl of RNA
653 template, yielding no amplification. RNA quality was determined on the Bioanalyser (Agilent)
654 with all yielding a RIN score of above 8. For each strain three independent RNA extractions
655 were made. A 5 µg aliquot of total RNA was depleted for rRNA with the mRNA then converted
656 into cDNA with the Scriptseq complete bacteria kit (Epicentre). The libraries were sequenced
657 on the Illumina HiSeq platform for 50 bp single end reads.

658

659 **RNA-seq data analysis**

660 RNA-seq data was analysed using the *S. aureus* USA300 FPR3757 reference genome
661 (accession number: NC_007793) and Kallisto [83], a kmer based pseudoalignment tool, with
662 analysis and visualization using Degust [https://github.com/drpowell/degust]. Degust uses
663 Voom/Limma [84] and generates an interactive website to analyse and explore the data.

664

665 **Preparation of samples for ChIP-seq**

666 An overnight culture (10 ml LB in 50 ml tube) of each strain NRS384Δ*spa* containing either
667 pRAB11: *walR*^{FLAG} / *vraR*^{FLAG} / *hptR*^{FLAG} / *saeR*^{FLAG} or pRAB11^{FLAG} only were grown at 37°C with
668 shaking at 200 rpm. Overnight cultures were diluted 1:100 in fresh LB (100 ml) in a 1 L baffled
669 flask and grown to an OD600nm of 0.5, induced with 100 ng/mL^{-1} of anhydrotetracycline and
670 grown for a further hour. Cells were crosslinked by direct addition of methanol free

671 formaldehyde (Pierce) to cultures (final concentration of 1% (v/v)) and incubated with gentle
672 mixing (rotating platform) for 15 min at room temperature. The crosslinking reaction was
673 quenched by addition of glycine to a final concentration of 400 mM and incubated a further
674 15 min. Cells were pelleted (7,000xg/10min/4°C), washed three times with ice-cold Phosphate
675 buffered saline (PBS) and the pellet stored at -80°C. For cell lysis, cells were suspended in 1ml
676 of lysis buffer (50 mM Tris-HCl [pH 7.4], 150 mM NaCl, 0.1% Triton X-100, 100 $\mu g/mL^{-1}$
677 lysostaphin (Ambi), 500 $\mu g/mL^{-1}$ RNaseA, complete mini protease inhibitor EDTA free
678 containing 100 um zirconium beads) and incubated for 20 min at 37°C. The weakened cells
679 were then disrupted using bead beating (6000 rpm for 1 min; Precellys 24 instrument) and
680 the cell lysate clarified by centrifugation (20,000*xg/*10min/4°C). The cation concentration of
681 the lysate was adjusted with $MgCl_2$ and $CaCl_2$ to 100 mM. The DNA was sheared by the
682 addition of a range of DNase I (NEB) concentrations (0.5 – 2U), in a 200 µL volume, followed
683 by incubation at 37°C for 10 min. The reaction was quenched by the addition of EDTA to 50
684 mM on ice. The degree of DNA fragmentation was assessed by electrophoresis of samples on
685 a 2% (v/v) agarose TAE gel. Samples showing maximal fragmentation at between 100-300 bp
686 were subjected to immunoprecipitation. Lysis buffer (made up to 4 ml - omitting lysostaphin
687 and RNase A) containing 10 µg of M2-anti FLAG antibody was added and incubated overnight
688 at 4°C on a rotating platform in a 15 ml tube. A 100 µl aliquot of Protein G agarose (Pierce)
689 was added to the lysate and incubated a further 2h at room temperature. The sample was
690 centrifuged (2,500*xg*/3 min/22°C) and the agarose pellet washed three time with 4 ml of IP
691 buffer (25mM Tris.Cl [pH 7.2], 150mM NaCl) and finally resuspended in 200 µl of elution
692 buffer (10mM Tris.Cl [pH 8], 1mM EDTA, 1% SDS containing 100µg of proteinase K). Crosslinks
693 were reversed incubation for 2h at 37°C and then 9h at 65°C with shaking at 1400 rpm. Finally,
694 eluted DNA was cleaned up by PCR purification (QiaQuick PCR purification kit, Qiagen). DNA

695 libraries were prepared with NEBNext® Ultra™ II DNA Library Prep Kit for Illumina and
696 sequenced using an Illumina MiSeq.

697

698 **ChIP-seq read mapping, peak identification, and motif searching.**

699 MiSeq reads from each of the five experiments (pRAB11: *walR*^{FLAG} / *vraR*^{FLAG} / *hptR*^{FLAG} /
700 *saeR*^{FLAG} or pRAB11^{FLAG} only) were first mapped to the *S. aureus* USA300 NC_007793 reference
701 chromosome using *samtools*. The resulting *.bam* and *.sam* files were used to create tag counts
702 (*i.e.,* mapped reads) with the *makeTagDirectory* script within *homer* [85]. The *homer* peak
703 identification tool (*findPeaks*) was extensively explored but high levels of background reads
704 were detected and precluded further use of *homer* for peak detection. An alternative strategy
705 was developed by building read coverage plots for viewing in Artemis [86], using *samtools* and
706 the command *% samtools depth -aa [target_file_name].bam [subtraction_file_name].bam |*
707 *cut -f3,4 | perl -nae 'use List::Util qw(max); print max(0, $F[0]-$F[1]),"\n";' >*
708 *[target_peaks].userplot*. This created a coverage plot of those regions of the *S. aureus* USA300
709 NC_007793 chromosome specifically bound by a given response regulator, relative the
710 response regulator sequence reads in the subtraction set. These subtraction sets were a
711 concatenation of a random selection of 20% of the sequence reads for the three response
712 regulators and the plasmid-only control combined. Thus, for peak discovery of WalR-binding
713 sites, an Artemis userplot was prepared from *vraR*^{FLAG} / *hptR*^{FLAG} / *saeR*^{FLAG} and pRAB11^{FLAG}
714 subtracted from *walR*^{FLAG}**.** The same method was used to generate userplots and discover
715 binding peaks for the remaining three response regulators. The '*create feature from graph*
716 *function*' in *Artemis* was then used to define chromosome regions represented by the
717 subtraction coverage plots. These regions were mapped to the NRS384 genome in Geneious

718 Prime (v2023.03) and searched using TGTNNNNNNNNTGT +/- 5bp as input. Output sequences
719 were combined with motif regions +/- 5bp for the following previously experimentally
720 validated WalR regulon members; SAUSA300_0739, SAUSA300_0955, SAUSA300_2051,
721 SAUSA300_2253, SAUSA300_2503 [12, 24] and input to WebLogo [87]. The resultant sequence logo
722 was converted to IUPAC code and used to search the NRS384 genome using Geneious Prime
723 (v2023.03).

724

725 **Mapping TSS in relation to WalR binding sites**

726 The *S. aureus* NRS384 genome was annotated in Geneious Prime (v2023.03) with predicted
727 transcriptional start sites (TSS) as defined in a previous study [39]. The 500 bp upstream of a
728 predicted TSS were extracted and manually annotated with -35 and -10 elements and
729 predicted WalR binding sites. T-tests (run in Stata v16.0) were used to test associations
730 between WalR binding site position and orientation, with gene expression data from RNA-
731 seq.

732

733 **Essentiality analysis**

734 Essentiality of *S. aureus* genes was called if a locus had been described as essential in two
735 previous studies [41, 42] and did not harbour a transposon insertion in the Nebraska transposon
736 library [43]. Genes were defined as belonging to the core genome if they were present in every
737 strain of the *Aureo*Wiki orthologue table (https://aureowiki.med.uni-
738 greifswald.de/download_orthologue_table)[88]. Data from RNA-seq, ChIP-seq, and the
739 essentiality and core genome analysis were integrated in R (v4.0.3, https://www.r-

740 project.org/) with RStudio 2022.02.0+443 using dplyr (v1.0.8) and tibble (v3.1.6), then
741 visualised using UpSetR (v1.4.0) [43] with ggplot2(v3.3.5).

742 **Growth curves, other phenotypic testing.**

743 For measurement of growth curves, *S. aureus* was grown overnight in BHI broth at 37°C and
744 subsequently diluted into fresh BHI broth to an $OD600_{nm}$ of 0.05. Growth was measured for 8
745 hours at 37°C with 300 rpm dual orbital shaking in a 96 well plate (Corning) using a Clariostar
746 Plus (BMG) plate reader.

747

748 **Antibacterial susceptibility testing**

749 Minimum inhibitory concentrations of antibacterial agents were determined by broth
750 microdilution; bacteria were exposed to 2-fold serial dilutions of antibacterial agents in
751 Mueller-Hinton broth 2 (BBL, BD) according to the guidelines provided by the Clinical and
752 Laboratory Standards Institute. Vancomycin susceptibility was assessed using gradient plates
753 as previously described [89].

754

755 **Lysostaphin sensitivity**

756 An overnight 5ml BHI culture of each strain was diluted 1:100 in an Eppendorf tube
757 containing fresh BHI containing different final concentrations (0 - 1.6 $\mu g/mL^{-1}$) of lysostaphin
758 (Ambi). Cells were then incubated statically for 90 min at 37°C in a water bath with the
759 CFU/mL^{-1} determined by dilution and spot plating onto BHI agar. Plates were incubated for 18 h
760 at 37°C before enumeration.

761 **LTA extraction, purification, and analysis by PAGE**

762 For extraction and analysis of LTA, 50 mL of LB was inoculated with a single colony of NRS384,
763 NRS384 Δ*yycHI,* NRS384 *walK*$_{T101A}$, NRS384 *walK*$_{T389A,}$ or RN4220, and grown at 37°C with
764 vigorous shaking for 18 h. Cells were harvested from 30 ml of saturated culture by
765 centrifugation of (5000 *x g*, 10 min) and LTA was extracted and analysed by PAGE as described
766 previously [90].

767

768 ***CRISPRi constructs and knockdown analysis.***

769 To generate pSD1 CRISPRi knockdown constructs for *walR, hla* and *hup,* primers
770 corresponding to the previously described for *walR* (IM1180/IM1181) and *hla*
771 (IM1182/IM1183) were synthesised from Zhao *et al* [91]. Knockdown primers for *hup* (targeted
772 the region overlapping and upstream of the *hup* start codon (IM1559/IM1560)) were
773 designed with the annealed primer pairs for *walR*, *hla* and *hup* cloned into the SapI site of
774 pSD1 as described previously [92]. Plasmids were then transformed into NRS384. Overnight
775 cultures (5ml LB, chloramphenicol 10 µg/mL^{-1} in 50 ml tubes) were then diluted in fresh media
776 1:100 containing different concentrations of aTc to induce expression of dCAS9, with the
777 optical density of the cultures followed.

778 RNA isolation: RNA was isolated from 1ml of cells (induced with either 0 or 100 ng/mL^{-1} of
779 aTc) after 5h of growth, as described above. A 1ug aliquot of total RNA was converted into
780 cDNA with Superscript IV and random hexamers as described previously [93]. For RT-qPCR, 1 µl
781 of cDNA was used as template with primers for *gyrB* (IM1020/IM1021), *hla* (IM1026/IM1027),
782 *walR* (IM1153/IM1154) and *hu* (IM1586/IM1587) with Luna Universal qPCR Master Mix (NEB)
783 on a Quantstudio 1 PCR machine. The data was normalised to the *gyrB* gene and analysed
784 with the ΔΔ CT method [94].

785 Plasmid isolation: Plasmid DNA was isolated from 10 ml of cells at 5h post induction (induced
786 with 0, 10, 50 and 100 ng/mL^{-1} aTc). Cells were centrifuged 7,000*xg*/2min pellet was washed
787 in 1ml of PBS and then resuspended in 400 µl of the resuspension buffer (Monarch Miniprep
788 kit – NEB) containing 50 µg of lysostaphin. The cells were lysed at 37°C for 30 min and then
789 processed following the kit instructions through one column with elution in 30 µl of elution
790 buffer. DNA was quantified with the Qubit BR DNA quantification kit and normalised to 15
791 ng/µl, with the normalised loading (150ng of purified plasmid) assessed on a 1% TAE gel.
792 Subsequent 1% agarose gels (in 2xTBE) containing 2.5 µg/mL^{-1} chloroquine were run as
793 described by Cameron *et al* [95]. Gels (10cm) were run at 10V for 16h which were washed twice
794 (30 min each wash) in dH_2O and then stained with Sybr Gold for 30 min and subsequently
795 imaged.

796 Genomic isolation: Genomic DNA was isolated from the equivalent of OD600nm of 5 after 5h
797 of growth (induced with 0 or 100 ng/mL aTc). The cell pellet was washed with 1ml of PBS and
798 resuspended in 90 µl of PBS containing 5 µl of 20 mg/mL^{-1} RNase A, 50 µg of lysostaphin and
799 100 µl of the tissue lysis buffer (Monarch Genomic DNA purification kit, NEB). Cells were lysed
800 at 37°C for 30 min and then processed following the manufactures instructions.

801 **Analysis of *ori-ter* ratios**

802 To measure to *ori-ter* ratios, genomic DNA prepared after CRISPRi knockdown (as above) was
803 sequenced using the Illumnia NextSeq (by the Doherty Applied Microbial Genomics facility,
804 University of Melbourne). Illumina reads were processed and analysed using iRep, as
805 previously described (v1.1 https://github.com/christophertbrown/iRep [96]).

806 ***Construction of pSmBIT and pLgBIT split luciferase vectors.***

807 The vector pRAB11(pC194 replicon) [34] was modified by PCR to restore the consensus *tetO*
808 upstream of the *tetR* gene (IM1290/IM1291) [97]. As described previously, this reduced the
809 impact of elevated level TetR production and allowed leaky expression of the target gene in
810 the absence of aTc. The above 6.4 kb PCR product was gel extracted, treated with SLiCE and
811 transformed into *E. coli* IM08B, yielding pRAB11*. To introduce a consensus ribosome binding
812 site and 9 nucleotide spacer before the start codon (AGGAGGAATTGGAAA) downstream of
813 the two *tetO* sites (proceeding the gene of interest), pRAB11* was first digested with KpnI
814 and gel extracted. This was used a template in a PCR (IM513/IM1355), the product digested
815 with KpnI, gel extracted and ligated. The ligation product was transformed into IM08B yielding
816 pRAB11*RBS. The *tetR**-RBS fragment was digested from pRAB11*RBS (SphI/KpnI) and
817 ligated into complementary digested pCN34 (pT181 replicon) [98] yielding pCN34*RBS. Both
818 pRAB11*RBS and pCN34*RBS were digested with KpnI, gel extracted and used as template in
819 a PCR (IM515/IM1356). The following combinations were combined with 50 ng of each 1.
820 pRAB11*RBS PCR and LINKER(GSSGGGGSGGGGSSG)-SmBIT gBlock. 2. pCN34*RBS PCR and
821 LINKER-LgBIT gBlock. gBlock sequences were codon optimised for *S. aureus* The SLiCE
822 reactions were transformed into IM08B yielding either pSmBIT or pLgBIT, with both vectors
823 were fully sequenced to validate.

824 ***Cloning into split luciferase vectors***

825 Either pSmBIT and pLgBIT were digested with KpnI, gel extracted and used as template for
826 PCR with primers IM515/IM1360. The pSmBIT or pLgBIT amplimers were combined with
827 amplified open reading frames with stop codon removed and tailed with 5'-
828 GATAGAGTATGATGAGGAGGAATTGGAAA-3' forward or 5'-GAACCACCACCACCACTAGAACC-3'
829 sequences complementary to the vector.

830 WalR and WalK alleles were PCR amplified with IM1363/IM1364 and IM1365/IM1366,
831 respectively, then SLiCE cloned into pSmBIT (for *walR* alleles) or pLgBIT (for *walK* alleles) and
832 transformed into IM08B. For *S. aureus* transformations, at least 1 µg of pLgBIT(+*walK* allele)
833 and pSmBIT(+ *walR* allele) were purified from IM08B and co-electroporated into NRS384 with
834 selection on BHI agar containing 10 ug/mL^{-1} chloramphenicol and 50 ug/mL^{-1} kanamycin.

835 ***Chromosomal tagging of WalR-SmBIT and WalK-LgBIT***

836 To access the functional interaction of WalR/WalK under native levels of protein of
837 production, the native copy on the chromosome was tagged with SmBIT for WalR and LgBIT
838 for WalK. The regions of DNA were assembled as follows. 1. *walR*-SmBIT-*walK*: *walR*-SmBIT
839 was amplified from pSmBIT-*walR* with IM107/IM1517 and a downstream fragment
840 encompassing *walK* was amplified with IM1516/IM10 from NRS384 genomic DNA. Both were
841 gel extracted and joined by SOE-PCR. 2. *walK*-LgBIT-*yycH*: *walK*-LgBIT was amplified from
842 pLgBIT-*walK* with IM7/IM1519 and a downstream fragment encompassing 500bp of *yycH* was
843 amplified with IM1518/IM44 on NRS384 genomic DNA. Both were gel extracted and joined
844 by SOE-PCR. Either amplimer was SLiCE cloned into pIMAY-Z and transformed into IM08B. The
845 above cloning steps and *S. aureus* allelic exchange was performed as described by Monk and
846 Stinear [79]. Presence of *walR*-SmBIT and *walK*-LgBIT were screened by colony PCR with
847 IM1360/IM1368 and IM1360/IM44, respectively. Genomic DNA was isolated from the strains
848 and whole genome sequenced.

849

850 ***Growth and luciferase curves***

851 An overnight 5 ml LB containing antibiotics (in a 50ml tube) were grown overnight. The culture
852 was diluted 1:100 in fresh LB supplemented with chloramphenicol and kanamycin including a
853 1:5000 dilution of the Nano-Glo® Luciferase Assay Substrate (Promega). Preliminary growth
854 curves in the presence of the substrate showed no impact on growth at this concentration.
855 The culture was then dispensed in triplicate (200 µl) black/clear bottom 96 well plates (Cat
856 no. 165305, Themofisher). The plates were sealed with MicroAmp™ Optical Adhesive Film
857 (Thermofisher) and incubated at 37°C with dual orbital shaking at 300 rpm (Clariostar Plus,
858 BMG). Every 10 minutes the plate was read at OD600nm and light emission (1s exposure)
859 collected over an 8 h period.

860 ***Bacterial luciferase reporter plasmid***

861 To construct pIMK1-LUX, the Listeria phage integrase vector pIMK was digested with
862 SphI/BglII to excise the PSA integrase and replace it with the PCR amplified (IM1241/IM1242)
863 low copy number pSK41 replicon from pLOW, yielding pIMK1. Vectors pIMK1 and pPL2*lux*
864 were then digested with SalI/PstI and the gel extracted pIMK1 backbone ligated to the
865 bacterial luciferase operon from pPL2*lux*. The vector pIMK1-LUX produces exact promoter
866 fusions which can be cloned into the SalI/SwaI digested vector, as described previously [99].
867 Promoters for *walR* (IM1222/IM32), *sasD* (IM1216/IM248 (Wt) or IM1217(ccc)), *sle1*
868 (IM1295/IM1115; IM1114/IM1296), *0602* (IM1294/IM1119; IM1118/IM1062), *ltaS*
869 (IM1218/IM1117; IM1116/IM1219), $ssaA^{CCCII}$ (IM1297/IM1121; IM1120/IM1298), $isaA^{CCCI}$
870 (IM1220/IM1123; IM1122/IM1221), $isaA^{CCCII}$ (IM1220/IM1125; IM1124/IM1221), *tarF*
871 (LS451/LS448; LS449/LS452), *tagG* (LS457/LS454; LS455/LS458), *dnaA* (IM1745/IM1744;
872 IM1743/IM1746), $dnaD^{CCCI}$ (LS471/LS466; LS467/LS472), $dnaD^{CCCII}$ (LS471/LS468;
873 LS469/LS472,) *rplK* (IM1734/LS143; LS144/IM1735), *hup* (IM1289/IM1290; IM1291/IM1292),

874 *dnaA*^{CCCI} (LS443/LS440; LS441/IM1746), *dnaA*^{CCCII} (LS443/LS438; LS439/IM1746), *dnaA*^{CCCIII}
875 (LS443/IM1743; IM1744/IM1746), and *prs* (IM1285/LS139; IM140/IM1288) were PCR
876 amplified from genomic DNA with either the outer set (Wt promoter) or SOE-PCR with the
877 four primers (ccc promoter). The amplimers were digested with SalI, gel extracted and cloned
878 into the above double digested vector. Plasmids isolated from IM08B were transformed into
879 NRS384 Wt. An overnight 5ml LB culture with kanamycin was diluted 1:100 in fresh LB
880 containing kanamycin with growth curves and light emission measured as described above
881 for the split luciferase with the substrate omitted.

882 **Data visualisation**

883 Graphs were generated in R (v4.0.3, https://www.r-project.org/)or GraphPad Prism (v9.3.1)
884 software packages.

885 **Data availability:** The DNA sequence reads for ChIP-seq and RNA-seq have been submitted to
886 the NCBI Gene Expression Omnibus (GEO) repository under accession number GSE212321.
887 DNA sequence reads for *ori-ter* analysis have been submitted to NCBI under Bioproject ID
888 PRJNA886746.

889 Acknowledgements

890 We are grateful to the following colleagues of for their advice, assistance, and input into this
891 work: Justin Clarke, Charlie Higgs, Danielle Ingle, Karinna Saxby. T.P.S. is supported by
892 NHMRC Research Grant (APP1105525) and NHMRC project grant GNT1145075. H. E. G. M. is
893 supported through an NHMRC ideas grant 2003192. A.M.T. is supported by an Australian
894 Government Research Training Program scholarship.

References

1. Care ACoSaQiH. AURA 2021: Fourth Australian report on antimicrobial use and resistance in human health. (2021).

2. Howden BP, Peleg AY, Stinear TP. The evolution of vancomycin intermediate Staphylococcus aureus (VISA) and heterogenous-VISA. *Infect Genet Evol* **21**, 575-582 (2014).

3. Bai AD*, et al.* Staphylococcus aureus bacteraemia mortality: a systematic review and meta-analysis. *Clin Microbiol Infect* **28**, 1076-1084 (2022).

4. Wozniak TM, Dyda A, Merlo G, Hall L. Disease burden, associated mortality and economic impact of antimicrobial resistant infections in Australia. *Lancet Reg Health West Pac* **27**, 100521 (2022).

5. Martin PK, Li T, Sun D, Biek DP, Schmid MB. Role in cell permeability of an essential two-component system in Staphylococcus aureus. *J Bacteriol* **181**, 3666-3673 (1999).

6. Delaune A, Poupel O, Mallet A, Coic YM, Msadek T, Dubrac S. Peptidoglycan crosslinking relaxation plays an important role in Staphylococcus aureus WalKR-dependent cell viability. *PLoS One* **6**, e17054 (2011).

7. Dubrac S, Msadek T. Identification of genes controlled by the essential YycG/YycF two-component system of Staphylococcus aureus. *J Bacteriol* **186**, 1175-1181 (2004).

8. Villanueva M*, et al.* Sensory deprivation in Staphylococcus aureus. *Nat Commun* **9**, 523 (2018).

9. Fabret C, Hoch JA. A two-component signal transduction system essential for growth of Bacillus subtilis: implications for anti-infective therapy. *J Bacteriol* **180**, 6375-6383 (1998).

10. Dubrac S, Msadek T. Tearing down the wall: peptidoglycan metabolism and the WalK/WalR (YycG/YycF) essential two-component system. *Adv Exp Med Biol* **631**, 214-228 (2008).

11. Howell A*, et al.* Genes controlled by the essential YycG/YycF two-component system of Bacillus subtilis revealed through a novel hybrid regulator approach. *Mol Microbiol* **49**, 1639-1655 (2003).

12. Dubrac S, Boneca IG, Poupel O, Msadek T. New insights into the WalK/WalR (YycG/YycF) essential signal transduction pathway reveal a major role in controlling cell wall metabolism and biofilm formation in Staphylococcus aureus. *J Bacteriol* **189**, 8257-8269 (2007).

13. Bisicchia P*, et al.* The essential YycFG two-component system controls cell wall metabolism in Bacillus subtilis. *Mol Microbiol* **65**, 180-200 (2007).

14. Cameron DR, Jiang JH, Kostoulias X, Foxwell DJ, Peleg AY. Vancomycin susceptibility in methicillin-resistant Staphylococcus aureus is mediated by YycHI activation of the WalRK essential two-component regulatory system. *Sci Rep* **6**, 30823 (2016).

15. Szurmant H, Mohan MA, Imus PM, Hoch JA. YycH and YycI interact to regulate the essential YycFG two-component system in Bacillus subtilis. *J Bacteriol* **189**, 3280-3289 (2007).

16. Fukuchi K, Kasahara Y, Asai K, Kobayashi K, Moriya S, Ogasawara N. The essential two-component regulatory system encoded by yycF and yycG modulates expression of the ftsAZ operon in Bacillus subtilis. *Microbiology (Reading)* **146 (Pt 7)**, 1573-1583 (2000).

17. Fukushima T, Furihata I, Emmins R, Daniel RA, Hoch JA, Szurmant H. A role for the essential YycG sensor histidine kinase in sensing cell division. *Mol Microbiol* **79**, 503-522 (2011).

18. Dubrac S, Bisicchia P, Devine KM, Msadek T. A matter of life and death: cell wall homeostasis and the WalKR (YycGF) essential signal transduction pathway. *Mol Microbiol* **70**, 1307-1322 (2008).

19. Fukushima T, Szurmant H, Kim EJ, Perego M, Hoch JA. A sensor histidine kinase co-ordinates cell wall architecture with cell division in Bacillus subtilis. *Mol Microbiol* **69**, 621-632 (2008).

20. Takada H*, et al.* Essentiality of WalRK for growth in Bacillus subtilis and its role during heat stress. *Microbiology (Reading)* **164**, 670-684 (2018).

21. Poupel O*, et al.* Transcriptional Analysis and Subcellular Protein Localization Reveal Specific Features of the Essential WalKR System in Staphylococcus aureus. *PLoS One* **11**, e0151449 (2016).

22. Dobihal GS, Brunet YR, Flores-Kim J, Rudner DZ. Homeostatic control of cell wall hydrolysis by the WalRK two-component signaling pathway in Bacillus subtilis. *Elife* **8**, (2019).

23. Monk IR*, et al.* Zinc-binding to the cytoplasmic PAS domain regulates the essential WalK histidine kinase of Staphylococcus aureus. *Nat Commun* **10**, 3067 (2019).

24. Delauné A*, et al.* The WalKR system controls major staphylococcal virulence genes and is involved in triggering the host inflammatory response. *Infect Immun* **80**, 3438-3453 (2012).

25. Rapun-Araiz B*, et al.* Systematic Reconstruction of the Complete Two-Component Sensorial Network in Staphylococcus aureus. *mSystems* **5**, (2020).

26. Libby EA, Goss LA, Dworkin J. The Eukaryotic-Like Ser/Thr Kinase PrkC Regulates the Essential WalRK Two-Component System in Bacillus subtilis. *PLoS Genet* **11**, e1005275 (2015).

27. Huynh TN, Noriega CE, Stewart V. Conserved mechanism for sensor phosphatase control of two-component signaling revealed in the nitrate sensor NarX. *Proc Natl Acad Sci U S A* **107**, 21140-21145 (2010).

28. Monk IR*, et al.* Zinc-binding to the cytoplasmic PAS domain regulates the essential WalK histidine kinase of Staphylococcus aureus. *Nature Communications* **10**, 3067 (2019).

29. Martin PK*, et al.* Novel locus required for expression of high-level macrolide-lincosamide-streptogramin B resistance in Staphylococcus aureus. *J Bacteriol* **184**, 5810-5813 (2002).

30. Buschiazzo A, Trajtenberg F. Two-Component Sensing and Regulation: How Do Histidine Kinases Talk with Response Regulators at the Molecular Level? *Annu Rev Microbiol* **73**, 507-528 (2019).

31. Wood A, Irving SE, Bennison DJ, Corrigan RM. The (p)ppGpp-binding GTPase Era promotes rRNA processing and cold adaptation in Staphylococcus aureus. *PLoS Genet* **15**, e1008346 (2019).

32. Hu J, Zhang X, Liu X, Chen C, Sun B. Mechanism of reduced vancomycin susceptibility conferred by walK mutation in community-acquired methicillin-resistant Staphylococcus aureus strain MW2. *Antimicrob Agents Chemother* **59**, 1352-1355 (2015).

33. Heilmann C, Hussain M, Peters G, Götz F. Evidence for autolysin-mediated primary attachment of Staphylococcus epidermidis to a polystyrene surface. *Mol Microbiol* **24**, 1013-1024 (1997).

34. Helle L*, et al.* Vectors for improved Tet repressor-dependent gradual gene induction or silencing in Staphylococcus aureus. *Microbiology (Reading)* **157**, 3314-3323 (2011).

35. Belcheva A, Verma V, Golemi-Kotra D. DNA-binding activity of the vancomycin resistance associated regulator protein VraR and the role of phosphorylation in transcriptional regulation of the vraSR operon. *Biochemistry* **48**, 5592-5601 (2009).

36. Sun F, Li C, Jeong D, Sohn C, He C, Bae T. In the Staphylococcus aureus two-component system sae, the response regulator SaeR binds to a direct repeat sequence and DNA binding requires phosphorylation by the sensor kinase SaeS. *J Bacteriol* **192**, 2111-2127 (2010).

37. Yang Y, Sun H, Liu X, Wang M, Xue T, Sun B. Regulatory mechanism of the three-component system HptRSA in glucose-6-phosphate uptake in Staphylococcus aureus. *Med Microbiol Immunol* **205**, 241-253 (2016).

38. Gründling A, Schneewind O. Synthesis of glycerol phosphate lipoteichoic acid in Staphylococcus aureus. *Proc Natl Acad Sci U S A* **104**, 8478-8483 (2007).

39. Prados J, Linder P, Redder P. TSS-EMOTE, a refined protocol for a more complete and less biased global mapping of transcription start sites in bacterial pathogens. *BMC Genomics* **17**, 849 (2016).

40. Sengupta M, Jain V, Wilkinson BJ, Jayaswal RK. Chromatin immunoprecipitation identifies genes under direct VraSR regulation in Staphylococcus aureus. *Can J Microbiol* **58**, 703-708 (2012).

41. Valentino MD*, et al.* Genes contributing to Staphylococcus aureus fitness in abscess- and infection-related ecologies. *mBio* **5**, e01729-01714 (2014).

42. Chaudhuri RR*, et al.* Comprehensive identification of essential Staphylococcus aureus genes using Transposon-Mediated Differential Hybridisation (TMDH). *BMC Genomics* **10**, 291 (2009).

43. Fey PD*, et al.* A genetic resource for rapid and comprehensive phenotype screening of nonessential Staphylococcus aureus genes. *mBio* **4**, e00537-00512 (2013).

44. Martin E*, et al.* DNA replication initiation in Bacillus subtilis: structural and functional characterization of the essential DnaA–DnaD interaction. *Nucleic Acids Research* **47**, 2101-2112 (2018).

45. Huang YH, Lien Y, Huang CC, Huang CY. Characterization of Staphylococcus aureus Primosomal DnaD Protein: Highly Conserved C-Terminal Region Is Crucial for ssDNA and PriA Helicase Binding but Not for DnaA Protein-Binding and Self-Tetramerization. *PLoS One* **11**, e0157593 (2016).

46. Buchad H, Nair M. The small RNA SprX regulates the autolysin regulator WalR in Staphylococcus aureus. *Microbiological Research* **250**, 126785 (2021).

47. Pang T, Wang X, Lim HC, Bernhardt TG, Rudner DZ. The nucleoid occlusion factor Noc controls DNA replication initiation in Staphylococcus aureus. *PLoS Genet* **13**, e1006908 (2017).

48. Percy MG, Gründling A. Lipoteichoic acid synthesis and function in gram-positive bacteria. *Annu Rev Microbiol* **68**, 81-100 (2014).

49. Kho K, Meredith TC. Salt-Induced Stress Stimulates a Lipoteichoic Acid-Specific Three-Component Glycosylation System in Staphylococcus aureus. *J Bacteriol* **200**, (2018).

50. Yao J, Zhong J, Fang Y, Geisinger E, Novick RP, Lambowitz AM. Use of targetrons to disrupt essential and nonessential genes in Staphylococcus aureus reveals temperature sensitivity of Ll.LtrB group II intron splicing. *RNA* **12**, 1271-1281 (2006).

51. Kim DH*, et al.* β-Arm flexibility of HU from Staphylococcus aureus dictates the DNA-binding and recognition mechanism. *Acta Crystallogr D Biol Crystallogr* **70**, 3273-3289 (2014).

52. Stojkova P, Spidlova P, Stulik J. Nucleoid-Associated Protein HU: A Lilliputian in Gene Regulation of Bacterial Virulence. *Front Cell Infect Microbiol* **9**, 159 (2019).

53. Rouvière-Yaniv J, Yaniv M, Germond J-E. E. coli DNA binding protein HU forms nucleosome-like structure with circular double-stranded DNA. *Cell* **17**, 265-274 (1979).

54. Karaboja X, Wang X. HBsu Is Required for the Initiation of DNA Replication in Bacillus subtilis. *J Bacteriol*, e0011922 (2022).

55. Karaboja X, Wang X. HBsu Is Required for the Initiation of DNA Replication in Bacillus subtilis. *J Bacteriol* **204**, e0011922 (2022).

56. Howden BP*, et al.* Evolution of multidrug resistance during Staphylococcus aureus infection involves mutation of the essential two component regulator WalKR. *PLoS Pathog* **7**, e1002359 (2011).

57. Wörmann ME, Reichmann NT, Malone CL, Horswill AR, Gründling A. Proteolytic cleavage inactivates the Staphylococcus aureus lipoteichoic acid synthase. *J Bacteriol* **193**, 5279-5291 (2011).

58. Kuroda M, Kuroda H, Oshima T, Takeuchi F, Mori H, Hiramatsu K. Two-component system VraSR positively modulates the regulation of cell-wall biosynthesis pathway in Staphylococcus aureus. *Mol Microbiol* **49**, 807-821 (2003).

59. Belcheva A, Golemi-Kotra D. A close-up view of the VraSR two-component system. A mediator of Staphylococcus aureus response to cell wall damage. *J Biol Chem* **283**, 12354-12364 (2008).

60. Fernandes PB, Reed P, Monteiro JM, Pinho MG. Revisiting the Role of VraTSR in Staphylococcus aureus Response to Cell Wall-Targeting Antibiotics. *J Bacteriol* **204**, e0016222 (2022).

61. Hancock IC. Bacterial cell surface carbohydrates: structure and assembly. *Biochem Soc Trans* **25**, 183-187 (1997).

62. Hesser AR, Schaefer K, Lee W, Walker S. Lipoteichoic acid polymer length is determined by competition between free starter units. *Proc Natl Acad Sci U S A* **117**, 29669-29676 (2020).

63. Barbuti MD, Myrbråten IS, Morales Angeles D, Kjos M. The cell cycle of Staphylococcus aureus: An updated review. *MicrobiologyOpen* **12**, e1338 (2023).

64. Gallay C*, et al.* CcrZ is a pneumococcal spatiotemporal cell cycle regulator that interacts with FtsZ and controls DNA replication by modulating the activity of DnaA. *Nature Microbiology* **6**, 1175-1187 (2021).

65. Karaboja X, Wang X. HBsu Is Required for the Initiation of DNA Replication in Bacillus subtilis. *J Bacteriol* **204**, e00119-00122 (2022).

66. Verma SC, Harned A, Narayan K, Adhya S. Non-specific and specific DNA binding modes of bacterial histone, HU, separately regulate distinct physiological processes through different mechanisms. *Mol Microbiol*, (2023).

67. Ohniwa RL, Ushijima Y, Saito S, Morikawa K. Proteomic analyses of nucleoid-associated proteins in Escherichia coli, Pseudomonas aeruginosa, Bacillus subtilis, and Staphylococcus aureus. *PLoS One* **6**, e19172 (2011).

68. Gupta M*, et al.* HupB, a nucleoid-associated protein of Mycobacterium tuberculosis, is modified by serine/threonine protein kinases in vivo. *J Bacteriol* **196**, 2646-2657 (2014).

69. Hardt P*, et al.* The cell wall precursor lipid II acts as a molecular signal for the Ser/Thr kinase PknB of Staphylococcus aureus. *International Journal of Medical Microbiology* **307**, 1-10 (2017).

70. Burnside K*, et al.* Regulation of hemolysin expression and virulence of Staphylococcus aureus by a serine/threonine kinase and phosphatase. *PLoS One* **5**, e11071 (2010).

71. Takada H, Yoshikawa H. Essentiality and function of WalK/WalR two-component system: the past, present, and future of research. *Biosci Biotechnol Biochem* **82**, 741-751 (2018).

72. Shah IM, Dworkin J. Induction and regulation of a secreted peptidoglycan hydrolase by a membrane Ser/Thr kinase that detects muropeptides. *Mol Microbiol* **75**, 1232-1243 (2010).

73. Tiwari S*, et al.* Two-Component Signal Transduction Systems of Pathogenic Bacteria As Targets for Antimicrobial Therapy: An Overview. *Frontiers in Microbiology* **8**, (2017).

74. Legland D, Arganda-Carreras I, Andrey P. MorphoLibJ: integrated library and plugins for mathematical morphology with ImageJ. *Bioinformatics* **32**, 3532-3534 (2016).

75. Laws M, Shaaban A, Rahman KM. Antibiotic resistance breakers: current approaches and future directions. *FEMS Microbiology Reviews* **43**, 490-516 (2019).

76. Tan S, Cho K, Nodwell JR. A defect in cell wall recycling confers antibiotic resistance and sensitivity in Staphylococcus aureus. *J Biol Chem* **298**, 102473 (2022).

77. Campbell J*, et al.* Synthetic lethal compound combinations reveal a fundamental connection between wall teichoic acid and peptidoglycan biosyntheses in Staphylococcus aureus. *ACS Chem Biol* **6**, 106-116 (2011).

78. Bilyk BL, Panchal VV, Tinajero-Trejo M, Hobbs JK, Foster SJ. An Interplay of Multiple Positive and Negative Factors Governs Methicillin Resistance in Staphylococcus aureus. *Microbiol Mol Biol Rev* **86**, e0015921 (2022).

79. Monk IR, Stinear TP. From cloning to mutant in 5 days: rapid allelic exchange in Staphylococcus aureus. *Access Microbiol* **3**, 000193 (2021).

80. Monk IR, Tree JJ, Howden BP, Stinear TP, Foster TJ. Complete Bypass of Restriction Systems for Major Staphylococcus aureus Lineages. *mBio* **6**, e00308-00315 (2015).

81. Studier FW. Protein production by auto-induction in high density shaking cultures. *Protein Expr Purif* **41**, 207-234 (2005).

82. Hsieh YW, Alqadah A, Chuang CF. An Optimized Protocol for Electrophoretic Mobility Shift Assay Using Infrared Fluorescent Dye-labeled Oligonucleotides. *J Vis Exp*, (2016).

83. Bray NL, Pimentel H, Melsted P, Pachter L. Near-optimal probabilistic RNA-seq quantification. *Nature Biotechnology* **34**, 525-527 (2016).

84. Law CW, Chen Y, Shi W, Smyth GK. voom: Precision weights unlock linear model analysis tools for RNA-seq read counts. *Genome Biol* **15**, R29 (2014).

85. Duttke SH, Chang MW, Heinz S, Benner C. Identification and dynamic quantification of regulatory elements using total RNA. *Genome Res* **29**, 1836-1846 (2019).

86. Carver T, Harris SR, Berriman M, Parkhill J, McQuillan JA. Artemis: an integrated platform for visualization and analysis of high-throughput sequence-based experimental data. *Bioinformatics* **28**, 464-469 (2012).

87. Crooks GE, Hon G, Chandonia JM, Brenner SE. WebLogo: a sequence logo generator. *Genome Res* **14**, 1188-1190 (2004).

88. Fuchs S*, et al.* AureoWiki- The repository of the Staphylococcus aureus research and annotation community. *Int J Med Microbiol* **308**, 558-568 (2018).

89. Lee JYH*, et al.* Global spread of three multidrug-resistant lineages of Staphylococcus epidermidis. *Nat Microbiol* **3**, 1175-1185 (2018).

90. Kho K, Meredith TC. Extraction and Analysis of Bacterial Teichoic Acids. *Bio-protocol* **8**, e3078 (2018).

91. Zhao C, Shu X, Sun B. Construction of a Gene Knockdown System Based on Catalytically Inactive (“Dead”) Cas9 (dCas9) in Staphylococcus aureus. *Applied and Environmental Microbiology* **83**, e00291-00217 (2017).

92. Pryor JM, Potapov V, Kucera RB, Bilotti K, Cantor EJ, Lohman GJS. Enabling one-pot Golden Gate assemblies of unprecedented complexity using data-optimized assembly design. *PLOS ONE* **15**, e0238592 (2020).

93. Wong Fok Lung T*, et al.* Staphylococcus aureus small colony variants impair host immunity by activating host cell glycolysis and inducing necroptosis. *Nat Microbiol* **5**, 141-153 (2020).

94. Livak KJ, Schmittgen TD. Analysis of relative gene expression data using real-time quantitative PCR and the 2(-Delta Delta C(T)) Method. *Methods* **25**, 402-408 (2001).

95. Cameron ADS, Stoebel DM, Dorman CJ. DNA supercoiling is differentially regulated by environmental factors and FIS in Escherichia coli and Salmonella enterica. *Molecular Microbiology* **80**, 85-101 (2011).

96. Brown CT, Olm MR, Thomas BC, Banfield JF. Measurement of bacterial replication rates in microbial communities. *Nat Biotechnol* **34**, 1256-1263 (2016).

97. Schleimer N*, et al.* Adaption of an Episomal Antisense Silencing Approach for Investigation of the Phenotype Switch of Staphylococcus aureus Small-Colony Variants. *Front Microbiol* **10**, 2044 (2019).

98. Charpentier E, Anton AI, Barry P, Alfonso B, Fang Y, Novick RP. Novel cassette-based shuttle vector system for gram-positive bacteria. *Appl Environ Microbiol* **70**, 6076-6085 (2004).

99. Bron PA, Monk IR, Corr SC, Hill C, Gahan CG. Novel luciferase reporter system for in vitro and organ-specific monitoring of differential gene expression in Listeria monocytogenes. *Appl Environ Microbiol* **72**, 2876-2884 (2006).